Hidden Markov Models for Radio Localization in Mixed LOS/NLOS Conditions

Carlo Morelli, Monica Nicoli, *Member, IEEE*, Vittorio Rampa, and Umberto Spagnolini, *Senior Member, IEEE*

***Abstract*—This paper deals with the problem of radio localization of moving terminals (MTs) for indoor applications with mixed line-of-sight/non-line-of-sight (LOS/NLOS) conditions. To reduce false localizations, a grid-based Bayesian approach is proposed to jointly track the sequence of the positions and the sight conditions of the MT. This method is based on the assumption that both the MT position *and* the sight condition are Markov chains whose state is hidden in the received signals [hidden Markov model (HMM)]. The observations used for the HMM localization are obtained from the power-delay profile of the received signals. In ultrawideband (UWB) systems, the use of the whole power-delay profile, rather than the total power only, allows to reach higher localization accuracy, as the power-profile is a *joint* measurement of time of arrival *and* power. Numerical results show that the proposed HMM method improves the accuracy of localization with respect to conventional ranging methods, especially in mixed LOS/NLOS indoor environments.**

***Index Terms*—Bayesian estimation, hidden Markov models (HMM), mobile positioning, source localization, tracking algorithms, ultrawideband (UWB) communications, wireless networks.**

I. Introduction

In wireless communication systems, localization of moving terminals (MT) is obtained through the measurement of propagation parameters related to the MT location [1]–[5]. Parameter estimation is performed by exchanging radio signals with L fixed access points (APs) placed in known positions. Typical propagation parameters are times of arrival (TOA), time differences of arrival (TDOA), angles of arrival (AOA), and received signal strength (RSS) [3]. The relationship between these parameters and the MT position are obtained either by analytical models or through field measurements (e.g., by RSS digital maps). Usually these models or measurements are exploited to estimate the MT-APs distances/directions; then localization is obtained by tri-($L = 3$) or multi-($L > 3$) lateration/angulation. The choice of the measurement type (e.g., TOA, TDOA, AOA, RSS, or digital maps) and the localization approach (e.g., centralized or distributed, traditional or cooperative, etc.) depends on the characteristics of the specific application (e.g., indoor or outdoor) and on the wireless infrastructure. The latter ranges from cellular networks [6]–[8], to local area networks (WLAN) [9], personal area networks (WPAN) or sensor networks (WSN) [10]–[12].

False localizations often arise in ranging methods; these unwanted effects are due to parameter estimation errors, mismodeling, oversimplified assumptions about the propagation environment, multipath effects, and non-line-of-sight (NLOS) conditions. In indoor scenarios characterized by dense multipath and/or NLOS conditions, these errors become more severe as ranging results in *apparent* or biased distances due to propagation over secondary paths. For these reasons, advanced localization methods need to be designed taking into account the existence of mixed LOS/NLOS conditions. The most common techniques exploit redundant measurements (i.e., large L) [13], merge different types of measure with data fusion techniques [2], [14], combine analytical models with maps of measurements [8], [3], or use Bayesian methods to estimate (i.e., track) the whole MT trajectory instead of estimating one position at a time [15]–[18].

Differently from band-limited wireless systems, such as cellular radio ones, wideband or ultrawideband (UWB) signals make high resolution (e.g., below 1 m) ranging applications feasible [10], [19], [20]. UWB systems [21], [22] are mainly intended for limited-range indoor applications. In this paper, we consider a UWB network with $L \geq 3$ fixed nodes (i.e., APs) placed in known positions and covering the area where the MT has to be localized. Accurate ranging could be obtained, in principle, by estimating TOA or TDOA from signals at the output of the chip matched filter (MF), relying on the high resolution of the UWB transmitted pulse. However, dense multipath and large delay spreading, often found in indoor environments, worsen the inherent high resolution of UWB ranging systems. In addition, multiuser access interference (MAI) introduces further signal degradation. In these conditions, the high sampling rate required by the above mentioned TOA-based methods does not necessarily imply high resolution ranging results, due to the rich multipath environment that prevents an accurate estimation of the first arrival delay. To improve the localization accuracy, we propose to track the MT position *directly* from RSS-delay profile measurements rather than the usual two-step localization approach (i.e., parameter estimation and position tracking). In addition, the sampling

Manuscript received August 23, 2005; revised April 27, 2006. This work was supported by the FIRB-VICOM project (http://www.vicom-project.it/) funded by the Italian Ministry of Education, University and Research (MIUR). Part of this work was presented at the IEEE International Conference on Acoustic, Speech, and Signal Processing, Philadelphia, PA,March 18-23,2005 . The associate editor coordinating the review of this paper and approving it for publication was Prof. Kung Yao.

C. Morelli was with the Dipartimento di Elettronica e Informazione, Politecnico di Milano, I-20133 Milan, Italy. He is now with Siemens, S.p.A., I-20060 Cassina de' Pecchi (Milan), Italy (e-mail: carlo.morelli@gmail.com).

M. Nicoli and U. Spagnoli are with the Dipartimento di Elettronica e Informazione, Politecnico di Milano, I-20133 Milan, Italy (e-mail: nicoli@elet.polimi.it; spagnoli@elet.polimi.it).

V. Rampa is with the Institute of Electronics, Computer and Telecommunication Engineering—National Research Council (I.E.I.I.T.-C.N.R.), I-20133 Milan, Italy (e-mail: rampa@elet.polimi.it).

Color versions of Figs. 9 and 18 available online at http://ieeexplore.ieee.org.

Digital Object Identifier 10.1109/TSP.2006.889978

interval used for the RSS-delay profile can be adapted to the spatial resolution required by the localization system and can be lower than the chip-rate [10].

Here, we propose a network-based localization system where the MT motion, modeled as an hidden Markov model (HMM) [23], is estimated by means of a grid-based Bayesian tracking method. The MT location is estimated by exploiting *all* the signals collected up to the current time instant over the L wireless links [24]. The estimation method is an adaptation of the detection/tracking algorithm (D/TA) [25], previously developed for delay tracking in remote sensing applications and here modified to the specific radio-localization problem. The D/TA is a forward-only algorithm that can work in real-time by maximizing the *a posteriori* probability of the hidden state given all the signals collected up to the current step. In order to cope with indoor propagation and reduce the estimate bias introduced by the multipath, the HMM has been adapted to take into account mixed LOS/NLOS conditions. The hidden Markov state is defined as the ensemble of the MT position and the LOS/NLOS conditions for all the L MT-AP links. The D/TA can jointly track both the position and the sight condition by exploiting the continuity information of the MT trajectory. The power delay profiles for the signals received over the L radio links are used to track the most likely state sequence. It is worth noticing that, unlike other Bayesian estimators such as the Kalman filter (KF) or the extended Kalman filter (EKF) [17], [18], this HMM-based approach does not rely on linearization and Gaussian assumptions, still preserving about the same computational complexity of the aforementioned algorithms.

To summarize, the original contributions provided in this paper with respect to other localization methods in the literature are: the ability to model and handle mixed LOS/NLOS conditions within a HMM Bayesian framework; the use of both the first-arrival RSS and the RSS-delay profile rather than the first-arrival RSS only (i.e., a scalar measurement). The use of RSS-delay profiles is motivated by the higher localization accuracy that can be reached using this type of measurement in wide-band systems (e.g., UWB systems), as the RSS profile is a *joint* measurement of TOA *and* power [26]. On the contrary, in narrow band systems (e.g., IEEE 802.11b standard for WLAN) it is preferable to exploit scalar RSS measurements [16]. In this paper, we focus on localization for UWB systems using RSS-profile observations, but the proposed HMM framework is flexible enough to incorporate other type of measurements. In particular, the extension to localization from scalar RSS observations is straightforward [27]. Also AOA measurements could be easily exploited in the case of receivers with antenna arrays.

The paper is organized as follows. The localization problem is introduced in Section II where the discrete-time signal model is defined for a multiuser UWB scenario. In this section, the RSS-delay profile method is discussed in both LOS and NLOS conditions. In Section III, a joint sight-position maximum likelihood estimation (MLE) algorithm is introduced. Due to its shortcomings, this algorithm becomes the starting point for the D/TA localization algorithm that is fully presented in Section IV along with its HMM Bayesian framework. The D/TA performance is evaluated in Section V, at first in a very simple scenario and then in a more complex environment. Section VI draws some conclusions.

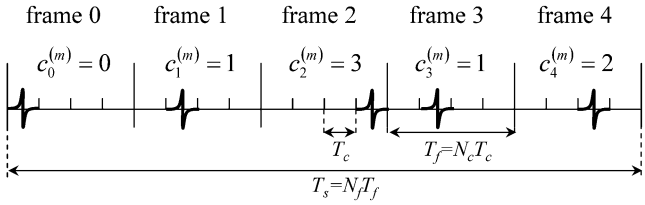

Fig. 1. Multiuser UWB transmission based on the BPSK antipodal signaling (TH-BPSK).

II. Problem Definition

A. UWB System Model

We consider an UWB uplink scenario where M active MTs transmit signals to the same AP using TH-BPSK modulation. Multiple access is handled by assigning different time-hopping (TH) codes to the active users; each user transmits data to the AP using binary-phase-shift-keying (BPSK) signaling. Though localization methods are here derived for this UWB framework, the ranging algorithms introduced in the following sections are independent from the specific modulation scheme. For instance, they may be applied also to TH systems with M-ary pulse position modulation (PPM) [20].

Within a single symbol interval T_s, the signal received at the AP is

$$r(t)=\sum_{m=1}^{M} b^{(m)}v^{(m)}(t)*h^{(m)}(t)+n(t) \tag{1}$$

where, for the mth user, the information-bearing symbol $b^{(m)}\in\{-1,+1\}$ modulates the TH signature $v^{(m)}(t)$; the channel impulse response $h^{(m)}(t)$ accounts for dense multipath effects while $n(t)$ is an additive white Gaussian noise (AWGN). In TH-BPSK systems, as depicted in Fig. 1, the symbol interval of length T_s consists of N_f frames, each having duration $T_f=T_s/N_f$ and being divided into N_c chips of length $T_c=T_f/N_c$.

The user-specific signature $v^{(m)}(t)$ is the superposition of N_f delayed pulses (one for each frame)

$$v^{(m)}(t)=\sum_{j=0}^{N_f-1} g_0\left(t-jT_f-c_j^{(m)}T_c\right) \tag{2}$$

having known waveform $g_0(t)$ with energy $E_g=1$ and delays selected according to the mth TH code $\mathbf{c}^{(m)}=[c_0^{(m)}\ \cdots\ c_{N_f-1}^{(m)}]$. Code chips $c_j^{(m)}\in\{0,1,\ldots,N_c-1\}$ are chosen (e.g., randomly or deterministically) to minimize the multiuser interference and avoid catastrophic collisions.

According to this multiuser scenario, we consider the localization of one user at a time. The signal used for the localization of the mth user is the output of the filter matched to the mth signature, $y^{(m)}(t)=r(t)*v^{(m)}(-t)$, evaluated within the frame

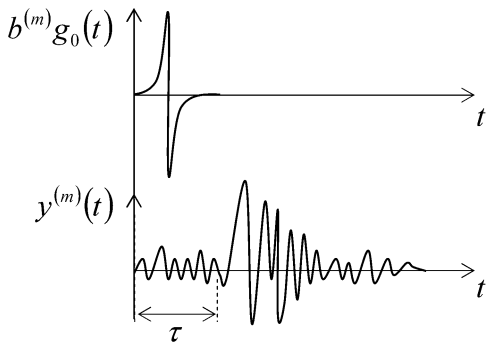

Fig. 2. Example of transmitted pulse (above) and received signal at the output of the pulse MF (below) for user m.

interval for $t \in [0, T_f]$. This can be equivalently written, apart from the normalizing factor $(1/N_f)$, as

$$y^{(m)}(t) = \frac{1}{N_f} \sum_{j=0}^{N_f-1} \int_{t+jT_f}^{t+(j+1)T_f} r(\tau) g_0 \left(\tau - jT_f - c_j^{(m)} T_c - t\right) d\tau. \tag{3}$$

From (1) and (2), it follows that:

$$y^{(m)}(t) = b^{(m)} g(t) * h^{(m)}(t) + w^{(m)}(t) = z^{(m)}(t) + w^{(m)}(t) \tag{4}$$

where $g(t) = g_0(t) * g_0(-t)$ is the convolution of the transmit and receive filters, $z^{(m)}(t) = b^{(m)} g(t) * h^{(m)}(t)$ is the signal contribution for the user of interest, while $w^{(m)}(t)$ gathers the interference from other users and the filtered background noise. Interference from adjacent symbols is not present as we simplified the signal model using only a single symbol. A typical example of pulse $g(t)$ used in UWB systems is the second-order derivative Gaussian pulse, $g(t) = [1 - (t/T_g)^2] \exp[-(1/2)(t/T_g)^2]$, with T_g denoting the half of the main lobe width, as sketched in the example of Fig. 2. The output (3) of the mth signature correlator could be equivalently obtained by first evaluating the UWB pulse matched filter $\tilde{r}(t) = r(t) * g_0(-t)$, then aligning (e.g., by compensating TH) and averaging the N_f frames according to $y^{(m)}(t) = (1/N_f) \sum_{j=0}^{N_f-1} \tilde{r}(t + jT_f + c_j^{(m)} T_c)$, as indicated in Fig. 3. The signal-to-noise ratio (SNR) in (4) depends on the number (K) of users and on the number (N_f) of combined frames.

B. Discrete-Time Signal Model

Let us now concentrate on the user of interest and drop the index m to simplify the notation. We sample the MF output $y(t) = z(t) + w(t)$ within the frame interval $t \in [0, T_f]$ at the sampling frequency $f_s = 1/\Delta t$, obtaining $K = \lceil T_f / \Delta t \rceil$ samples

$$y[k] = y((k-1)\Delta t) = z[k] + w[k], \quad k = 1, \ldots, K. \tag{5}$$

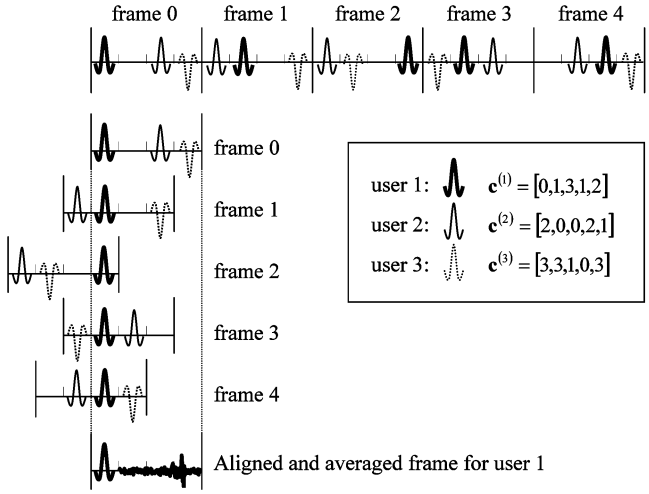

Fig. 3. Example of multiuser UWB TH-BPSK transmission aligned frames.

The sampling interval Δt is chosen as a tradeoff between the resolution required by the localization system and the limited computational power available at the APs. Since the target here is not the estimation of all the multipath delays, but rather of the first arrival from RSS measurements (i.e., any energy-related indicators), the choice of Δt is not necessarily constrained by the sampling theorem for the signal $y(t)$ [28].

By gathering all the K samples, the K-dimensional measurement vector $\mathbf{y}$ is defined as

$$\mathbf{y} = [y[1] \cdots y[K]]^{\mathrm{T}} = \mathbf{z} + \mathbf{w} \tag{6}$$

in terms of the K-dimensional vectors $\mathbf{z} = [z[1] \cdots z[K]]^{\mathrm{T}}$ and $\mathbf{w} = [w[1] \cdots w[K]]^{\mathrm{T}}$. As widely assumed in the literature (see, e.g., [29], [30]), the noise-plus-interference vector $\mathbf{w}$ is approximated as AWGN with known variance σ_0^2, i.e., $\mathbf{w} \sim \mathcal{N}(\mathbf{0}, \sigma_0^2 \mathbf{I}_K)$ with $\mathbf{I}_K$ denoting the $K \times K$ identity matrix. We recall from (4) that the information-bearing signal $\mathbf{z}$ depends on the channel response $h(t)$. Before focusing on localization, we need to make some simplifying assumptions about $h(t)$ to describe and handle propagation effects in dense multipath environments. The channel is, thus, modeled as the superposition of N_p paths, characterized by uncorrelated fading amplitudes $\{\alpha(p)\}_{p=1}^{N_p}$ and times of delay $\{\tau(p)\}_{p=1}^{N_p}$

$$h(t) = \sum_{p=1}^{N_p} \alpha(p) \delta(t - \tau(p) \cdot \Delta t) \tag{7}$$

where $\delta(t)$ is the Dirac's delta function. Delays are assumed to be multiple of the sampling interval Δt and to cover the whole temporal support for $[\tau(1), K]$: $\tau(p) = \tau(1) + p - 1$ for $p = 1, \ldots, K - \tau(1) + 1$. We also model the amplitudes $\{\alpha(p)\}$ as a zero-mean Gaussian random process with an exponentially decaying power delay profile. Sight condition is specified according the parameter $s \in \{0, 1\}$ that is defined as $s = 0$ for LOS and $s = 1$ for NLOS scenarios. For localization, we are particularly concerned about the delay of the first arrival $\tau(1)$, that can be rewritten in terms of the LOS delay τ, the sight condition s between MT and AP and the additional NLOS delay δ.

In fact, the first arrival delay $\tau(1)$ equals the propagation time $\tau = d/(c\Delta t)$ over the MT-AP distance d in case of LOS, while it is increased by $\Delta\tau = s\delta = \delta > 0$ in case of NLOS

$$\tau(1) = \tau + \Delta\tau = \frac{d}{c\Delta t} + s\delta = \begin{cases} \frac{d}{c\Delta t} & \text{for } s = 0 \text{ (LOS)} \\ \frac{d}{c\Delta t} + \delta & \text{for } s = 1 \text{ (NLOS)} \end{cases} \quad (8)$$

where c represents the propagation velocity.

Recalling from (4) that $z(t) = b \cdot g(t) * h(t)$, it follows that sampled signal $\mathbf{z}$ may be rewritten as

$$\mathbf{z} = b \sum_{p=1}^{N_p} \alpha(p)\mathbf{g}(\tau(p)) \quad (9)$$

where the $K \times 1$ vector $\mathbf{g}(\tau(p))$

$$[\mathbf{g}(\tau(p))]_{k,1} = g((k-1)\Delta t - \tau(p)\Delta t) \quad k = 1, \ldots, K \quad (10)$$

gathers the samples of the pulse waveform $g(t)$ delayed by $\tau(p)$. According to the aforementioned assumptions, the signal (9) is a zero-mean Gaussian vector, $\mathbf{z} \sim \mathcal{N}(\mathbf{0}, \mathbf{C}_z(\tau, \Delta\tau))$, with covariance matrix $\mathbf{C}_z(\tau, \Delta\tau)$. The overall signal (6) is then $\mathbf{y} \sim \mathcal{N}(\mathbf{0}, \mathbf{C}(\tau, \Delta\tau))$ with covariance matrix $\mathbf{C}(\tau, \Delta\tau) = \sigma_0^2\mathbf{I}_K + \mathbf{C}_z(\tau, \Delta\tau)$ that not only depends on the LOS delay τ but also on the NLOS excess delay δ as the overall signal power is distributed over the time interval $\tau + \Delta\tau \le k \le K$. Here, the covariance matrix $\mathbf{C}_z(\tau, \Delta\tau)$ is assumed to be diagonal

$$\mathbf{C}_z(\tau, \Delta\tau) = \mathrm{diag}(P_z(\tau, \Delta\tau, 1), \ldots, P_z(\tau, \Delta\tau, K)) \quad (11)$$

with elements $P_z(\tau, \Delta\tau, k) = \mathrm{E}[|z[k]|^2]$ accounting for the power delay profile (PDP). In case of correlation of the sampled signals (e.g., due to the finite bandwidth of the pulse waveform $g(t)$), a prewhitening filtering can be performed before localization [26]. The power of the multipath arrivals is assumed to change along the delay axis k according to the filtered Poisson process model [31]

$$P_z(\tau, \Delta\tau, k) = \sigma_z^2(\tau)\rho^{k-\tau}u(k - \tau - \Delta\tau) \quad (12)$$

where the step function $u(k)$ is defined as $u(k) = 1$ for $k \ge 0$ and $u(k) = 0$ elsewhere. The signal power is thus assumed to be non-null only for $k \ge \tau + \Delta\tau$ and to decay exponentially from the first arrival power $\sigma_z^2(\tau)$ with the attenuation factor ρ expressed as

$$\rho = \exp\left[-\frac{\Delta t}{\tau_{\mathrm{rms}}}\right] < 1 \quad (13)$$

where τ_{rms} is the channel delay spread expressed in seconds.

To account for the dependence of the RSS on the propagation distance $d = c\tau\Delta t$, the power $\sigma_z^2(\tau)$ is assumed to decrease with the LOS delay τ according to the path-loss law

$$\sigma_z^2(\tau) = \sigma_{\mathrm{ref}}^2\left(\frac{d}{d_{\mathrm{ref}}}\right)^{-\alpha} = \sigma_{\mathrm{ref}}^2\left(\frac{\tau}{\tau_{\mathrm{ref}}}\right)^{-\alpha} \quad (14)$$

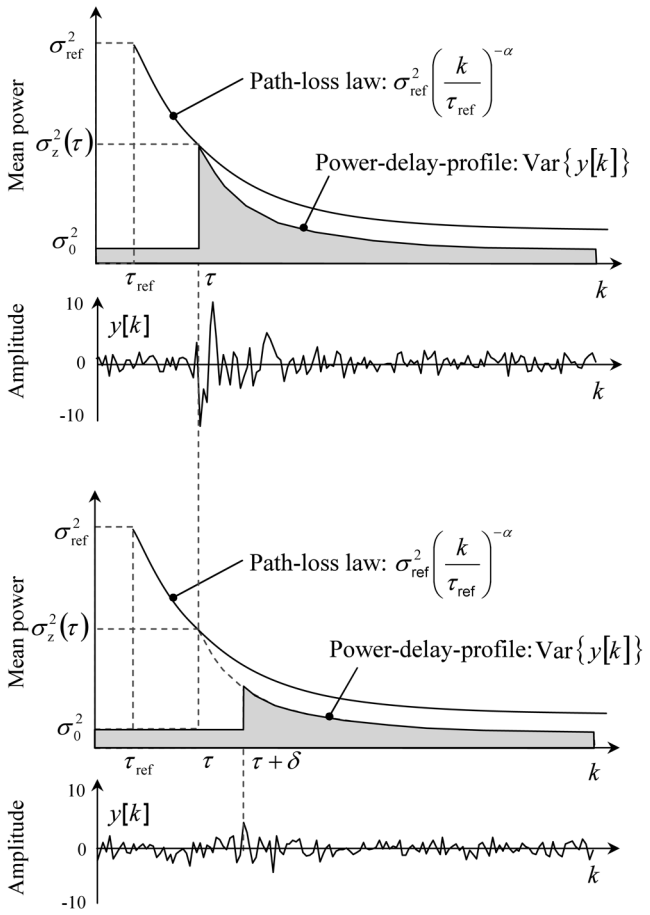

Fig. 4. RSS-profile model for LOS $s = 0$ (top) and NLOS $s = 1$ (bottom). The power of the signal sample $y[k]$ varies along the delay axis k according to the path-loss law and the exponential PDP for $k \ge \tau$. In case of NLOS, the PDP is windowed for $k \ge \tau + \delta$ due to the delay increment δ.

being $\sigma_{\mathrm{ref}}^2 = \sigma_z^2(\tau_{\mathrm{ref}})$ the power received at the reference distance $d_{\mathrm{ref}} = c\tau_{\mathrm{ref}}\Delta t$ and α the path-loss exponent (e.g., typical values are $\alpha = 2 \div 8$). The SNR is defined accordingly as

$$\eta(\tau) = \frac{\sigma_z^2(\tau)}{\sigma_0^2} = \eta_{\mathrm{ref}} \cdot \left(\frac{\tau}{\tau_{\mathrm{ref}}}\right)^{-\alpha} \quad (15)$$

with $\eta_{\mathrm{ref}} = \sigma_{\mathrm{ref}}^2/\sigma_0^2$ denoting the SNR at the reference distance d_{ref}. Examples of PDPs for LOS ($s = 0$) and NLOS ($s = 1$) cases are illustrated in Fig. 4. In these examples, the signal component is superimposed to the noise only for $k \ge \tau + \Delta\tau$, with $\Delta\tau = 0$ in the LOS case Fig. 4(a) and $\Delta\tau = \delta > 0$ in the NLOS case Fig. 4(b).

Based on the signal model described above, in the next sections we will investigate how to improve localization robustness against multipath and NLOS effects. It is worth noticing that, in real-world channels, the accuracy of RSS-based localization is also worsened by shadowing fluctuations (due to obstructions such as furniture, walls, buildings, etc.). The effects of random shadowing on indoor localization have been investigated by the authors in a WSN scenario [27]. The localization approach therein considered is a simplified version of the HMM method here described but based on RSS measurements only. On the contrary, in this paper, both RSS and PDP measurements

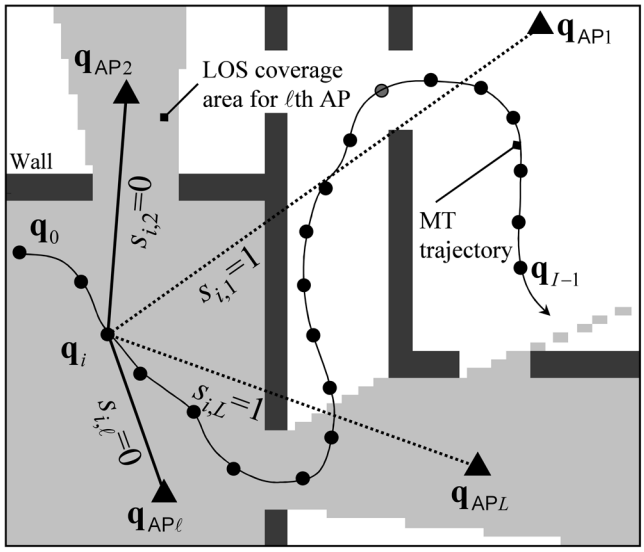

Fig. 5. Example of indoor localization by wireless infrastructure.

are considered, but shadowing is not included in the channel model. The extension to shadowing channels is still possible by modeling $\sigma_z^2(\tau)$ as a log-normal random variable and modifying the distribution of the measured signal $\mathbf{y}$ accordingly. Propagation models including shadowing effects for PDP-based localization can be found in [32] for indoor and [33] for outdoor environments.

C. Localization Problem

Let us now assume the indoor scenario depicted in Fig. 5, where the MT moves within an area covered by an UWB network with $L \geq 3$ fixed APs. The MT has to be localized from the radio signals exchanged within the UWB infrastructure. We assume a synchronous network where the APs are perfectly synchronized so that estimated delays can be directly used for ranging; if not, additional synchronization can be performed as described in [34]. Signals transmitted by the MT are received by all the APs and used to estimate the MT position every T_0 seconds (in practical systems, T_0 includes several symbol intervals). At time instants iT_0, for $i = 0, 1, \ldots, I-1$, the ℓth AP extracts location information from the received signal and forward them to a central monitoring unit (CMU) that is responsible for localization of the MT.

The position of each AP is known by the CMU and it is indicated as $\mathbf{q}_{\mathrm{AP}\ell} = [q_{\mathrm{AP}\ell}(1), q_{\mathrm{AP}\ell}(2)] \in \mathcal{Q}$, with $q_{\mathrm{AP}\ell}(1)$ and $q_{\mathrm{AP}\ell}(2)$ denoting the spatial coordinates of the ℓth AP ($\ell = 1, \ldots, L$) over the two-dimensional (2-D) space $\mathcal{Q}$. To simplify the layout, we assume that $\mathcal{Q}$ is a regular squared grid (with spatial sampling interval Δq) where each position is indicated by $\mathbf{n} = [n_1, n_2]$, with $n_1 \in \{0, \ldots, N_1 - 1\}$ and $n_2 \in \{0, \ldots, N_2 - 1\}$. The MT is characterized, at the ith time instant, by the unknown spatial position $\mathbf{q}_i = [q_i(1), q_i(2)] \in \mathcal{Q}$ and the unknown sight conditions $\mathbf{s}_i = [s_{i,1} \cdots s_{i,L}] \in \mathcal{S}$ with respect to all L APs, where $\mathcal{S} = \{0, 1\}^L$ is the set collecting the 2^L possible LOS/NLOS combinations for $\mathbf{s}_i$. Each sight condition is a binary random variable: $s_{i,\ell} = 0$ for LOS or $s_{i,\ell} = 1$ for NLOS.

According to the signal model introduced in Section II-B, the signal

$$\mathbf{y}_{i,\ell} = \mathbf{z}_{i,\ell} + \mathbf{w}_{i,\ell} \tag{16}$$

received by the ℓth AP at the ith time instant is modeled as a nonstationary zero-mean Gaussian vector $\mathbf{y}_{i,\ell} \sim \mathcal{N}(\mathbf{0}, \mathbf{C}(\tau_{i,\ell}, \Delta\tau_{i,\ell}))$ with covariance matrix $\mathbf{C}(\tau_{i,\ell}, \Delta\tau_{i,\ell})$ depending on the PDP of the ℓth channel. The PDP is related to the propagation time over the ℓth MT-AP distance $d_{i,\ell} = \|\mathbf{q}_i - \mathbf{q}_{\mathrm{AP}\ell}\|$ (e.g., expressed in spatial samples)

$$\tau_{i,\ell} = \frac{\|\mathbf{q}_i - \mathbf{q}_{\mathrm{AP}\ell}\|}{\bar{c}} \tag{17}$$

and to the NLOS excess delay $\Delta\tau_{i,\ell} = s_{i,\ell}\delta_{i,\ell} \geq 0$. Here the velocity $\bar{c}$ is normalized with respect to the sampling intervals: $\bar{c} = c\Delta t/\Delta q$. The unknown excess delay $\delta_{i,\ell} > 0$ is modeled as a random variable with known distribution $f_\delta(k) = p(\delta_{i,\ell} = k)$. In this paper, exponential distribution will be considered but other choices are possible [32], [33]. The SNR is defined according to (15) as $\eta(\tau_{i,\ell}) = \eta_{\mathrm{ref}} \cdot (\tau_{i,\ell}/\tau_{\mathrm{ref}})^{-\alpha}$.

The overall set of all L measurements used at time instant i for the localization is the $KL \times 1$ signal vector $\mathbf{y}_i = [\mathbf{y}_{i,1}^{\mathrm{T}}, \ldots, \mathbf{y}_{i,L}^{\mathrm{T}}]^{\mathrm{T}}$. According to the received signal power model (12)–(15), the overall RSS profile depends on the sight conditions $\{s_{i,\ell}\}_{\ell=1}^L$, the LOS propagation times $\{\tau_{i,\ell}\}_{\ell=1}^L$ and the additional NLOS delays $\{\delta_{i,\ell}\}_{\ell=1}^L$: the power of the kth sample $P_y(\tau_{i,\ell}, \Delta\tau_{i,\ell}, k) = \mathrm{E}[|y_{i,\ell}[k]|^2]$ is indeed

$$P_y(\tau_{i,\ell}, \Delta\tau_{i,\ell}, k) = \begin{cases} \sigma_0^2 & k < \tau_{i,\ell} + s_{i,\ell}\delta_{i,\ell} \\ \sigma_0^2 \left[1 + \eta_{\mathrm{ref}} \left(\frac{\tau_{i,\ell}}{\tau_{\mathrm{ref}}}\right)^{-\alpha} \rho^{k-\tau_{i,\ell}}\right] & k \geq \tau_{i,\ell} + s_{i,\ell}\delta_{i,\ell}. \end{cases} \tag{18}$$

It follows that the measurement vector $\mathbf{y}_i$ depends not only on the L distances between the MT and the APs, but it is also affected by the sight conditions $\mathbf{s}_i$. Accurate localization is therefore feasible (provided that $L \geq 3$) from RSS-profile measurements if NLOS conditions are taken into account.

As shown in Fig. 4, the first arrival represents an abrupt change in the second order statistics (18) of the measured signal, thus it will be indicated in the next paragraphs as the *breakpoint* (BP) event. In case of LOS conditions (i.e., $s_{i,\ell} = 0$), the BP delay and power are related to the MT-AP distance $d_{i,\ell}$. It is therefore possible to estimate the MT location $\mathbf{q}_i$ from $\mathbf{y}_i$, by a separate estimation (or ranging) of each distance $d_{i,\ell}$ from the measurement $\mathbf{y}_{i,\ell}$ for $\ell = 1, \ldots, L$, then followed by a tri- or multilateration of $\{d_{i,\ell}\}_{\ell=1}^L$ (e.g., for $L = 3$ or $L > 3$, respectively). This approach is the mostly adopted in the literature, though the measurement used for ranging is usually the total RSS and not the RSS profile along the delay axis. Scalar RSS is often adopted to save processing capabilities but it is known to be not very accurate (e.g., due to shadowing effects) unless very short-distance scenarios are adopted [35]. As an example, this approach has been adopted in [27] for radio localization in WSN.

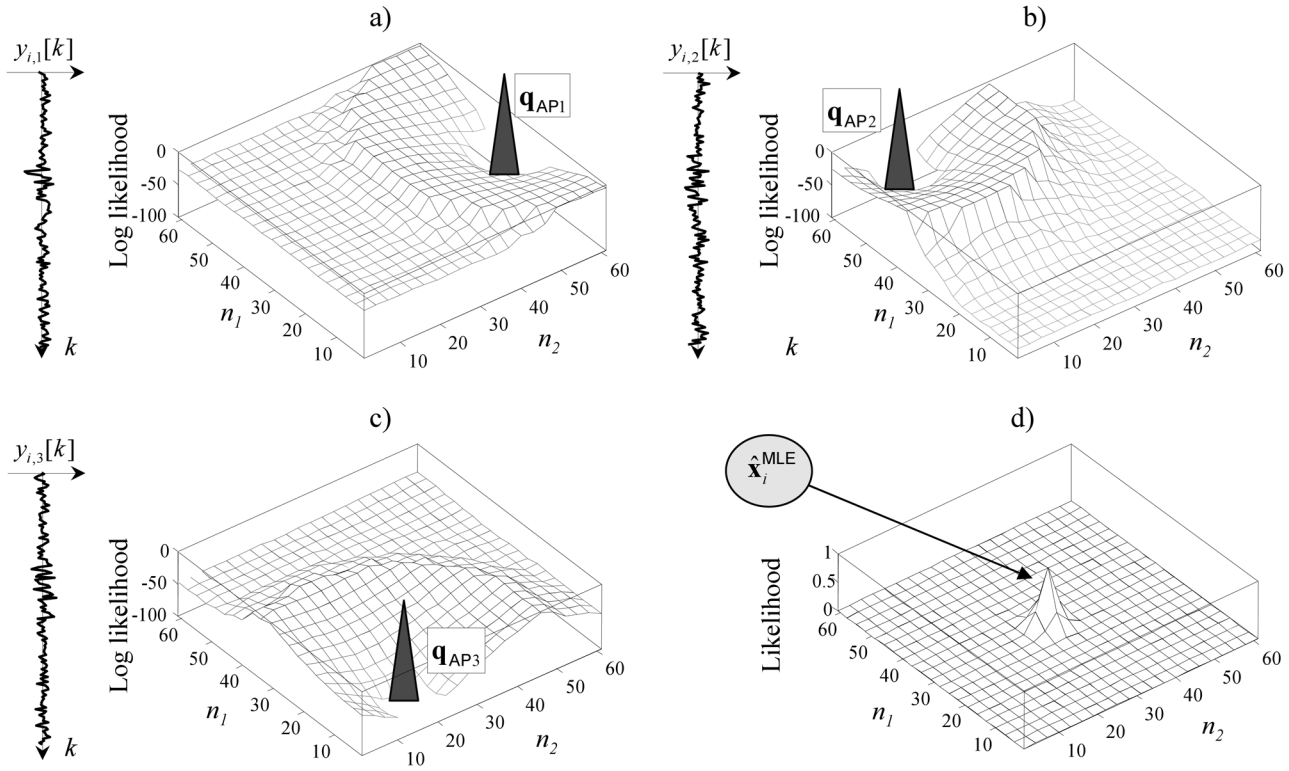

Fig. 6. Example of log-likelihood functions for the signal $\mathbf{y}_i$ measured from $L = 3$ APs in LOS conditions ($\mathbf{s}_i = \mathbf{0}$): the ranging pdf $p(\mathbf{y}_{i,\ell} \,|\, \mathbf{q}_i = \mathbf{n}, s_{i,\ell} = 0)$ for $\ell = 1, 2, 3$ (in logarithmic scale) and the position pdf $p(\mathbf{y}_i \,|\, \mathbf{q}_i = \mathbf{n}, \mathbf{s} = \mathbf{0})$ are indicated in (a), (b), (c), and (d), respectively. The position pdf is obtained by multiplying the L marginal pdfs. Likelihood functions are normalized for visualization purposes.

In this paper, we propose a novel localization approach where the location $\mathbf{q}_i$ is *directly* estimated (i.e., without preliminary ranging) from the measured signals $\{\mathbf{y}_i\}$ by exploiting the memory of the MT trajectory (i.e., by MT tracking). In Section III, we will introduce the MLE of $\mathbf{q}_i$ based on the current measurement $\mathbf{y}_i$ without tracking. The shortcoming of this "memory-less" approach is the high number of false localizations occurring in NLOS conditions as shown in Section V. In fact, in LOS situations, the BP is related to the true MT-AP distance $d_{i,\ell}$ while, in NLOS scenarios it depends on the apparent distances $d_{i,\ell} + \Delta d_{i,\ell}$, where the bias $\Delta d_{i,\ell} = \bar{c}\delta_{i,\ell} > 0$ is due to the propagation over reflected paths. The key idea is to solve this problem by *jointly* tracking the position $\mathbf{q}_i$ *and* the sight conditions $\mathbf{s}_i$ using the whole set of observations $\mathbf{y}_{0:i} = \{\mathbf{y}_0, \ldots, \mathbf{y}_i\}$ up to the current instant i.

The HMM method developed in Section IV is based on the assumption that *both* the mobile position $\mathbf{q}_i$ *and* the L link sight conditions $\mathbf{s}_i$ are Markov chains whose state is hidden in the measured signals $\mathbf{y}_i$ and must be *jointly* recovered keeping into account the continuity of the MT trajectory as sketched in Fig. 5. Joint estimation of $\mathbf{q}_i$ and $\mathbf{s}_i$ is performed by using a first-order HMM tracking algorithm that is able to manage mixed LOS/NLOS conditions.

III. Local ML Estimation From RSS Profiles

Let us assume that the joint position-sight variable $\mathbf{x}_i = (\mathbf{q}_i, \mathbf{s}_i)$ takes values in the finite set $\mathcal{X} = \mathcal{Q} \times \mathcal{S}$ of $2^L N_1 N_2$ elements. In this section, we consider the estimation of $\mathbf{x}_i$ from the signals measured only at the generic time instant i (i.e., *local estimation only*) using the maximum likelihood (ML) approach. The local MLE from the L-link measurement $\mathbf{y}_i$ is obtained by maximizing the likelihood function

$$\hat{\mathbf{x}}_i^{(\mathrm{MLE})} = \underset{\mathbf{x}_i \in \mathcal{X}}{\arg\max}\ p(\mathbf{y}_i \,|\, \mathbf{x}_i). \tag{19}$$

For any $\mathbf{n} = [n_1, n_2] \in \mathcal{Q}$ and $\mathbf{k} = [k_1, \ldots, k_L] \in \mathcal{S}$, the L observations $\{\mathbf{y}_{i,\ell}\}_{\ell=1}^{L}$ conditioned to the position $\mathbf{q}_i = \mathbf{n}$ and sight conditions $\mathbf{s}_i = \mathbf{k}$ are statistically independent. Hence, the likelihood function $p(\mathbf{y}_i \,|\, \mathbf{x}_i = (\mathbf{n}, \mathbf{k}))$ for all links simplifies to the product of the marginal probabilities for each link

$$p(\mathbf{y}_i \,|\, \mathbf{q}_i = \mathbf{n}, \mathbf{s}_i = \mathbf{k}) = \prod_{\ell=1}^{L} p(\mathbf{y}_{i,\ell} \,|\, \mathbf{q}_i = \mathbf{n}, s_{i,\ell} = k_\ell). \tag{20}$$

For $s_{i,1} = \cdots = s_{i,L} = 0$, an example is given in Fig. 6 where it is illustrated how multi-lateration is implicitly performed in the evaluation of the joint probability (20) without the need of a preliminary ranging phase.

According to the Gaussian assumptions for the signal model defined in Section II-B, the conditioned probability, given the LOS delay τ and the additional NLOS delay $\Delta\tau = s\delta$, is

$$\Lambda(\mathbf{y}, \tau, \Delta\tau) = |\,\mathbf{C}(\tau, \Delta\tau)\,|^{-1/2}(2\pi)^{-K/2} \times \exp\left[-\frac{1}{2}\mathbf{y}^{\mathrm{T}}\mathbf{C}^{-1}(\tau, \Delta\tau)\mathbf{y}\right]. \tag{21}$$

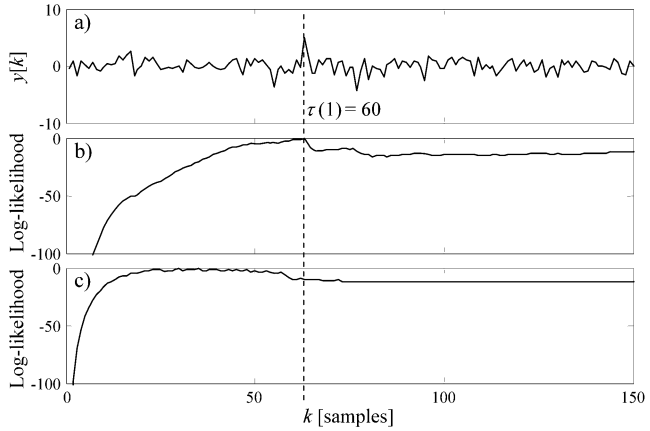

Fig. 7. Evaluation of the likelihood function for a single AP (the AP index is dropped). (a) Measured signal $y[k]$ ($\tau = 50$, $s = 1$, $\delta = 10$). (b) Log-likelihood function in LOS. (c) Log-likelihood function in NLOS. Likelihood functions are normalized for visualization purposes.

The ℓth likelihood function $p(\mathbf{y}_{i,\ell} \,|\, \mathbf{q}_i = \mathbf{n}, s_{i,\ell} = k_\ell)$ in (20) can now be easily rewritten as a function of $\Lambda(\mathbf{y}, \tau, \Delta\tau)$. For $k_\ell = 0$, it becomes

$$p(\mathbf{y}_{i,\ell} \,|\, \mathbf{q}_i = \mathbf{n}, s_{i,\ell} = 0) = \Lambda\left(\mathbf{y}_{i,\ell}, \frac{\|\mathbf{n} - \mathbf{q}_{\mathrm{AP}\ell}\|}{\bar{c}} 0\right) \quad (22)$$

while for $k_\ell = 1$ it is

$$\begin{aligned} &p(\mathbf{y}_{i,\ell} \,|\, \mathbf{q}_i = \mathbf{n}, s_{i,\ell} = 1) \\ &\quad = \sum_{\delta} f_\delta(\delta) p(\mathbf{y}_{i,\ell} \,|\, \mathbf{q}_i = \mathbf{n}, s_{i,\ell} = 1, \delta_{i,\ell} = \delta) \\ &\quad = \sum_{\delta} f_\delta(\delta) \Lambda\left(\mathbf{y}_{i,\ell}, \frac{\|\mathbf{n} - \mathbf{q}_{\mathrm{AP}\ell}\|}{\bar{c}}, \delta\right). \end{aligned} \quad (23)$$

Examples of marginal pdf for LOS and NLOS are given in Fig. 7.

For large SNR ($\sigma_z^2(\tau) \gg \sigma_0^2$), the expression of the likelihood function (21) can be simplified by approximating the diagonal elements of $\mathbf{C}(\tau, \Delta\tau)$ in (18) according to

$$P_y(\tau, \Delta\tau, k) \approx \begin{cases} \sigma_0^2 & k < \tau + \Delta\tau \\ \sigma_1^2(\tau)\rho^{k-\tau} & k \geq \tau + \Delta\tau \end{cases} \quad (24)$$

where $\sigma_1^2(\tau) = \sigma_0^2 + \sigma_z^2(\tau)$. Using the approximation $\eta(\tau) \approx \sigma_1^2(\tau)/\sigma_0^2$, in the LOS case ($s = 0$) the conditioned probabilities (21) reduce to

$$\Lambda(\mathbf{y}, \tau, 0) \approx \frac{\beta[K - \tau, \eta(\tau)]}{(\sigma_0\sqrt{2\pi})^K} \exp\left[-\frac{E_0(\tau)}{2\sigma_0^2} - \frac{E_1(\tau)}{2\sigma_1^2(\tau)}\right] \quad (25)$$

where $\beta(u, v) = (\rho^{(u-1/4)} v^{(1/2)})^{-u}$ and

$$E_0(\tau) = \sum_{k=1}^{\tau} y^2[k] \quad (26)$$

$$E_1(\tau) = \sum_{k=\tau+1}^{K} y^2[k] \rho^{-(k-\tau)}. \quad (27)$$

These expressions denote the *backward* $E_0(\tau)$ and the *forward* signal energy $E_1(\tau)$ of the two parts of the measurement $\mathbf{y}$ segmented by the BP value τ. Similarly, in the NLOS case, ($s = 1$) we get

$$\Lambda(\mathbf{y}, \tau, \delta) \approx \Lambda(\mathbf{y}, \tau, 0)\Gamma(\mathbf{y}, \tau, \delta) \quad (28)$$

with $\Gamma(\mathbf{y}, \tau, \delta)$ given by

$$\begin{aligned} \Gamma(\mathbf{y}, \tau, \delta) = &\frac{1}{\beta(\delta, \eta(\tau))} \\ &\times \exp\left[-\frac{E_0(\tau + \delta) - E_0(\tau)}{2\sigma_0^2}\right. \\ &\left. - \frac{\rho^{-\delta} E_1(\tau + \delta) - E_1(\tau)}{2\sigma_1^2(\tau)}\right]. \end{aligned} \quad (29)$$

IV. HMM Tracking From RSS Profiles

A. HMM Definition

Aim of the HMM algorithm is the MT localization at each time instant i; this is accomplished considering not only the current measurement $\mathbf{y}_i$ but *all* measurements $\mathbf{y}_{0:i}$ collected over the MT trajectory up to the current instant. The HMM state is defined as the joint position-sight variable $\mathbf{x}_i = (\mathbf{q}_i, \mathbf{s}_i) \in \mathcal{X}$ already introduced in Section III. The state is hidden in the L-link observation vector $\mathbf{y}_i$

$$\mathbf{y}_i = \mathbf{f}(\mathbf{q}_i, \mathbf{s}_i) + \mathbf{w}_i \quad (30)$$

where $\mathbf{f}(\cdot, \cdot)$ denotes the vector of nonlinear functions describing the relationship between the position-sight state $(\mathbf{q}_i, \mathbf{s}_i)$ and the signal $\mathbf{z}_i = [\mathbf{z}_{i,1}^{\mathrm{T}}, \ldots, \mathbf{z}_{i,L}^{\mathrm{T}}]^{\mathrm{T}} = \mathbf{f}(\mathbf{q}_i, \mathbf{s}_i)$, while $\mathbf{w}_i = [\mathbf{w}_{i,1}^{\mathrm{T}}, \ldots, \mathbf{w}_{i,L}^{\mathrm{T}}]^{\mathrm{T}}$ is the overall measurement noise. Both the MT position $\mathbf{q}_i$ and the L sight conditions $\mathbf{s}_i$ are modeled as independent first-order homogeneous Markov chains. We also define an additional zero state, $\mathbf{x}_i = \mathbf{0}$, to indicate the absence of the MT signal (e.g., to account for measurements heavily affected by noise preventing any MT detection or for no MT at all). The overall set of states is then $\mathcal{X}_0 = \mathcal{X} \cup \{\mathbf{0}\}$ with cardinality $2^L N_1 N_2 + 1$.

In order to characterize the Markov chain $\mathbf{x}_i$, indicated in the next paragraphs as $\mathbf{x}_i \sim \mathcal{MC}(\boldsymbol{\pi}, \mathbf{A})$, we need to define the initial state probabilities $\boldsymbol{\pi} = \{p(\mathbf{x}_0)\}$ and the transition probabilities $\mathbf{A} = \{p(\mathbf{x}_i \,|\, \mathbf{x}_{i-1})\}$. Since the Markov state is hidden in the observations $\mathbf{y}_i$, we also have to assign the observation pdf $\mathbf{B} = \{p(\mathbf{y}_i \,|\, \mathbf{x}_i)\}$; these probabilities compose the overall HMM parameter set named $\boldsymbol{\lambda} = (\mathbf{A}, \mathbf{B}, \boldsymbol{\pi})$ for short.

Within the 2-D space $\mathcal{Q}$, the MT trajectory at time i is indicated by the set $\mathbf{q}_{0:i} = \{\mathbf{q}_0, \ldots, \mathbf{q}_i\}$. It is generated by the homogeneous Markov chain $\mathbf{q}_i \sim \mathcal{MC}(\boldsymbol{\pi}^{(q)}, \mathbf{A}^{(q)})$ according to

$$\mathbf{q}_i = \mathbf{q}_{i-1} + \mathbf{v}_i \quad (31)$$

where $\mathbf{v}_i$ is the 2-D discrete-time driving process with known distribution $f_{\mathbf{v}}(\mathbf{n}) = p(\mathbf{v}_i = \mathbf{n})$. The $(N_1 N_2)^2$ transition probabilities $\mathbf{A}^{(q)} = \{a_{\mathbf{m},\mathbf{n}}^{(q)}\}$ are calculated from (31) as

$$a_{\mathbf{m},\mathbf{n}}^{(q)} = p(\mathbf{q}_i = \mathbf{n} \,|\, \mathbf{q}_{i-1} = \mathbf{m}) \propto f_{\mathbf{v}}(\mathbf{n} - \mathbf{m}) \quad (32)$$

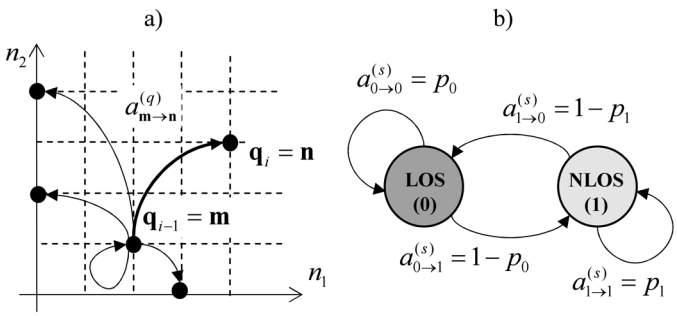

Fig. 8. First-order Markov models for position and sight. (a) Transition probabilities between the $N_1 N_2$ states of the position $\mathbf{q}_i$. (b) Transition probabilities between the two states of the sight condition $s_{i,\ell}$ for each MT-AP link.

for $\mathbf{m}, \mathbf{n} \in \mathcal{Q}$ [see Fig. 8(a)]. Examples of distribution $f_{\mathbf{v}}(\mathbf{n})$ and resulting trajectories $\mathbf{q}_{0:I-1}$ are given in Fig. 9. The form of the distribution $f_{\mathbf{v}}(\mathbf{n})$ is related to the features of the MT movement. For instance, a spiky shape, as the one shown in Fig. 9(c), indicates that the MT position is likely to remain confined around the current position. On the contrary, a flat distribution $f_{\mathbf{v}}(\mathbf{n})$ means that the MT position may have abrupt direction changes [e.g., Fig. 9(a)]. The initial-state distribution is defined as $\boldsymbol{\pi}^{(q)} = \{p(\mathbf{q}_0)\}$. Notice that, as shown in the examples of Fig. 9, the matrix $\mathbf{A}^{(q)}$ is sparse, thus reducing both memory storage and the effective computational power required for processing.

The sight condition variable $\mathbf{s}_i$ is also modeled as the first-order homogeneous Markov chain $\mathbf{s}_i \sim \mathcal{MC}(\boldsymbol{\pi}^{(s)}, \mathbf{A}^{(s)})$ with initial-state pdf $\boldsymbol{\pi}^{(s)} = \{p(\mathbf{s}_0)\}$ and transition probabilities $\mathbf{A}^{(s)} = \{a^{(s)}_{\mathbf{h},\mathbf{k}}\}$ where $a^{(s)}_{\mathbf{h},\mathbf{k}} = p(\mathbf{s}_i = \mathbf{k} \,|\, \mathbf{s}_{i-1} = \mathbf{h})$ and $\mathbf{h}, \mathbf{k} \in \mathcal{S}$ [e.g., Fig. 8(b)]. These parameters are calculated by assuming all the L sight conditions as i.i.d. first-order Markov chains with transition probabilities $a^{(s)}_{h,k} = p(s_{i,\ell} = k \,|\, s_{i-1,\ell} = h)$ for $h, k \in \{0, 1\}$. The probabilities to remain in the LOS or NLOS state are $p_0 = a^{(s)}_{0,0}$ or $p_1 = a^{(s)}_{1,1}$, respectively. Due to probability normalization, it is also $a^{(s)}_{0,1} = 1 - p_0$ and $a^{(s)}_{1,0} = 1 - p_1$. Notice that the parameters p_0 and p_1 do not depend on the index ℓ (i.e., the sight transition probabilities are the same for all the APs). Furthermore, for the APs independence, the transition probabilities for the overall sight process $\mathbf{s}_i$ are

$$a^{(s)}_{\mathbf{h},\mathbf{k}} = p(\mathbf{s}_i = \mathbf{k} \,|\, \mathbf{s}_{i-1} = \mathbf{h}) = \prod_{\ell=1}^{L} a^{(s)}_{h_\ell,k_\ell} \tag{33}$$

for each $\mathbf{h} = [h_1, \ldots, h_L], \mathbf{k} = [k_1, \ldots, k_L] \in \mathcal{S}$.

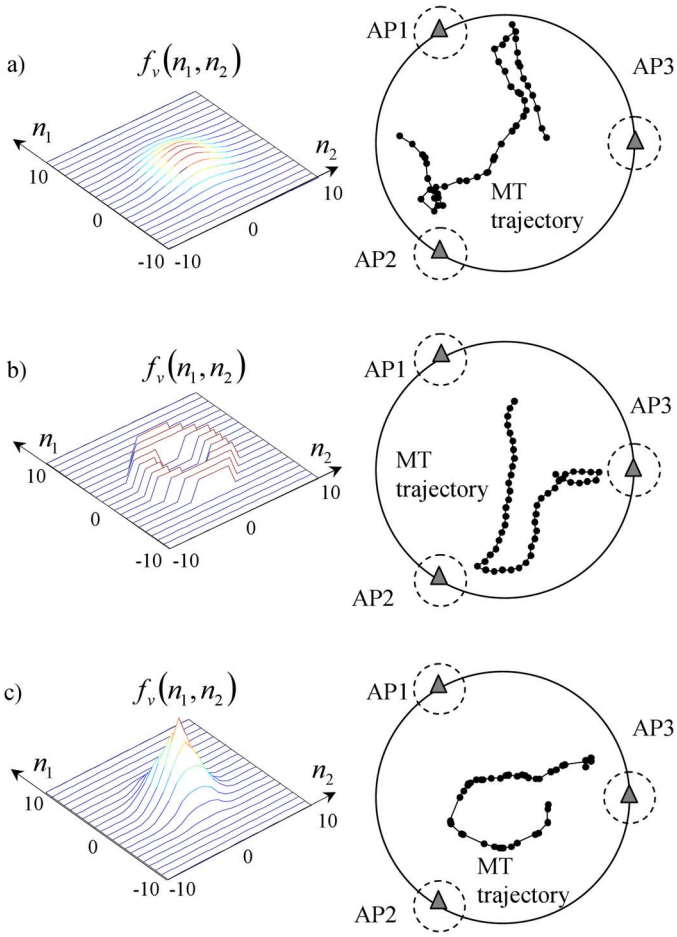

Fig. 9. Examples of 2-D pdf $f_v(\mathbf{n})$ for the random driving process $\mathbf{v}_i$. (a) Circular Gaussian pdf with deviation $\sigma_v = 3$ spatial samples. (b) Uniform ring with inner radius $r_1 = 3$ and external radius $r_2 = 5$ samples. (c) Cone with base having radius $\epsilon = 4$ samples. Notice that a large $f_v(\mathbf{0})$ value indicates that the MT is frequently still [as in (a) and (c)].

According to the independence assumption for $\mathbf{q}_i$ and $\mathbf{s}_i$, the probabilities of transition between nonzero states can now be calculated (apart from a normalizing factor) as

$$\begin{aligned} a^{(qs)}_{(\mathbf{m},\mathbf{h}),(\mathbf{n},\mathbf{k})} &= p(\mathbf{x}_i = (\mathbf{n},\mathbf{k}) | \mathbf{x}_{i-1} = (\mathbf{m},\mathbf{h})) \\ &= a^{(q)}_{\mathbf{m},\mathbf{n}} \cdot a^{(s)}_{\mathbf{h},\mathbf{k}} \end{aligned} \tag{34}$$

for $\mathbf{m}, \mathbf{n} \in \mathcal{Q}$ and $\mathbf{h}, \mathbf{k} \in \mathcal{S}$. On the other hand, transitions involving the zero state are ruled by the probabilities of trajectory initiation (ϑ) and termination (ν), both considered independent parameters. The whole set $\mathbf{A}$ of $(2^L N_1 N_2 + 1)^2$ transition probabilities is given by (35), shown at the bottom of the page. The term $\Gamma_{(\mathbf{m},\mathbf{h})}$ is used to normalize to 1 the sum of the transition

$$p(\mathbf{x}_i \,|\, \mathbf{x}_{i-1}) = \begin{cases} 1-\vartheta & \text{for } \mathbf{x}_{i-1} = \mathbf{x}_i = \mathbf{0} \\ \vartheta(2^L N_1 N_2)^{-1} & \text{for } \mathbf{x}_{i-1} = \mathbf{0}, \mathbf{x}_i = (\mathbf{n},\mathbf{k}) \\ \nu & \text{for } \mathbf{x}_{i-1} = (\mathbf{m},\mathbf{h}), \mathbf{x}_i = \mathbf{0} \\ (1-\nu) a^{(qs)}_{(\mathbf{m},\mathbf{h}),(\mathbf{n},\mathbf{k})} \Gamma_{(\mathbf{m},\mathbf{h})} & \text{for } \mathbf{x}_{i-1} = (\mathbf{m},\mathbf{h}), \mathbf{x}_i = (\mathbf{n},\mathbf{k}). \end{cases} \tag{35}$$

probabilities from each state, in order to avoid edge effects [25] at the borders of the finite grid $\mathcal{X}_0$.

The initial-state distribution is defined by assigning the $2^L N_1 N_2 + 1$ prior probabilities $\boldsymbol{\pi}$, i.e., by assigning the probabilities for the position ($\boldsymbol{\pi}^{(q)}$), the sight ($\boldsymbol{\pi}^{(s)}$) and the null state ($p(\mathbf{x}_0 = \mathbf{0})$) at time instant $i = 0$. A reasonable assignment in case of missing *a priori* information might be $p(\mathbf{x}_0) = 1/(2^{L+1} N_1 N_2)$ for $\mathbf{x}_i \neq \mathbf{0}$ and $p(\mathbf{x}_0) = 1/2$ for $\mathbf{x}_0 = \mathbf{0}$. Other initializations can be used when some *a priori* knowledge is available about the MT position $\mathbf{q}_0$ and the sight conditions $\mathbf{s}_0$.

We recall that the observation employed in this HMM framework is the real-valued $KL \times 1$ measurement vector $\mathbf{y}_i$, whose conditioned pdf $p(\mathbf{y}_i \,|\, \mathbf{x}_i)$ was evaluated in Section III for $\mathbf{x}_i = (\mathbf{n}, \mathbf{k})$. Having included the zero state in the set of states, to completely define the pdf set $\mathbf{B}$ we only need to compute the probability of the observation conditioned to $\mathbf{x}_i = \mathbf{0}$

$$p(\mathbf{y}_i \,|\, \mathbf{x}_i = \mathbf{0}) = \prod_{\ell=1}^{L} \Lambda(\mathbf{y}_{i,\ell}, K, 0). \tag{36}$$

In the following section, we will consider the estimation of the state sequence $\mathbf{x}_{0:I-1} = \{\mathbf{x}_0, \ldots, \mathbf{x}_{I-1}\}$ from the observations $\mathbf{y}_{0:I-1}$ under the assumption of known HMM parameter set $\boldsymbol{\lambda}$.

B. Detection/Tracking Algorithm

Given the model defined earlier, the optimal state sequence $\mathbf{x}_{0:I-1}$ associated with the ordered set of measurements $\mathbf{y}_{0:I-1}$ can be obtained using different estimation methods from the HMM theory [23]. Methods based on global criteria estimate all states $\mathbf{x}_{0:I-1}$ from the whole set of observations $\mathbf{y}_{0:I-1}$. Specifically, maximum-*a posteriori* state-by-state estimation can be obtained by maximizing for each state $\mathbf{x}_i$ the *a posteriori* pdf $p(\mathbf{x}_i | \mathbf{y}_{0:I-1}, \boldsymbol{\lambda})$ evaluated through the backward/forward algorithm (BFA). Alternatively, the Viterbi algorithm (VA) provides a method to select the optimum state sequence $\mathbf{x}_{0:I-1}$ that maximizes $p(\mathbf{x}_{0:I-1} | \mathbf{y}_{0:I-1}, \boldsymbol{\lambda})$. However, both BFA and VA are not suited for real-time localization, due to the unfeasible computational complexity and the latency in the state estimation. Therefore, we consider for localization a forward-only procedure that estimates $\mathbf{x}_i$ based on all measurements $\mathbf{y}_{0:i}$ collected up to the ith time instant.

The *Detection/Tracking Algorithm* (D/TA) is a Bayesian approach developed by the authors for an UWB radar system [37] and used in other different application frameworks [25]. Here, this algorithm is employed to estimate the position-sight state $\mathbf{x}_i = (\mathbf{q}_i, \mathbf{s}_i)$ by maximizing, over the whole state set $\mathcal{X}_0$, the *a posteriori* pdf $\gamma_i(\mathbf{x}_i) = p(\mathbf{x}_i \,|\, \mathbf{y}_{0:i}, \boldsymbol{\lambda})$ given the measurements $\mathbf{y}_{0:i}$ up to the current ith step

$$\hat{\mathbf{x}}_i^{\mathrm{D/TA}} = \arg\max_{\mathbf{x}_i \in \mathcal{X}_0} \gamma_i(\mathbf{x}_i). \tag{37}$$

The *a posteriori* pdf at time i is evaluated using the Bayes' theorem

$$\gamma_i(\mathbf{x}_i) = \mu_i \, p(\mathbf{y}_i \,|\, \mathbf{x}_i) p(\mathbf{x}_i \,|\, \mathbf{y}_{0:i-1}, \boldsymbol{\lambda}) \tag{38}$$

where $\forall i = 0, 1, \ldots, I-1$, the normalization term μ_i is defined such that $\sum_{\mathbf{x}_i \in \mathcal{X}_0} \gamma_i(\mathbf{x}_i) = 1$. The conditioned probability $p(\mathbf{y}_i \,|\, \mathbf{x}_i)$ is obtained from the current measurement vector $\mathbf{y}_i$ as described in Section IV-A, while the updating probability $p(\mathbf{x}_i \,|\, \mathbf{y}_{0:i-1}, \boldsymbol{\lambda})$ is calculated from the *a posteriori* pdf at the previous step

$$\gamma_{i-1}(\mathbf{x}_{i-1}) = p(\mathbf{x}_{i-1} \,|\, \mathbf{y}_{0:i-1}, \boldsymbol{\lambda}) \tag{39}$$

throughout the transition probabilities of the Markov chain

$$p(\mathbf{x}_i \,|\, \mathbf{y}_{0:i-1}, \boldsymbol{\lambda}) = \sum_{\mathbf{x}_{i-1} \in \mathcal{X}_0} p(\mathbf{x}_i \,|\, \mathbf{x}_{i-1}) \gamma_{i-1}(\mathbf{x}_{i-1}). \tag{40}$$

From (38) and (40), we get the forward recursion shown in (41) at the bottom of the page, that allows us to compute $\gamma_i(\mathbf{x}_i)$ for all scans from $i = 0$ up to $i = I-1$. In the first scan, the *a posteriori* pdf is initialized by $\gamma_0(\mathbf{x}_0)$ using the *a priori* distribution $p(\mathbf{x}_0)$.

Different approaches may be adopted to handle tracking termination and re-initialization when the MT signal gets too noisy or unreliable. For instance, in [37] the two hypotheses "detection" and "no detection" are defined as, respectively, $\mathbf{x}_i = \mathbf{0}$ and $\mathbf{x}_i \in \mathcal{X}$. To discriminate between these two conditions the comparison $\gamma_i(\mathbf{x}_i = \mathbf{0}) \gtrless \sum_{\mathbf{x}_i \in \mathcal{X}} \gamma_i(\mathbf{x}_i)$ or equivalently $\gamma_i(\mathbf{x}_i = \mathbf{0}) \gtrless 1/2$ is performed. In case of "no detection" the algorithm is reinitialized to the prior distribution $p(\mathbf{x}_0)$ (e.g., as in the first step $i = 0$). Otherwise (i.e., in case of "detection") the position-sight state is estimated using the MAP criterion over the nonzero states only: $\hat{\mathbf{x}}_i = \arg\max_{\mathbf{x}_i \in \mathcal{X}} \gamma_i(\mathbf{x}_i)$.

As far as the computational complexity is concerned, the number of multiplications required by the estimation of a HMM state sequence is in the order of $N^2 I$, with N denoting the number of states and I the sequence length. For the specific application herein considered, the number of states is $N = 2^L N_1 N_2 + 1$, which might lead to unfeasible computational burden for practical localization systems, such as WSN [11], [12]. However, it should be noticed that the dynamic model driving the MT motion is such to make the $N_1 N_2 \times N_1 N_2$ matrix $\mathbf{A}^{(q)}$ largely sparse. In fact, this matrix depends on the 2-D filtering kernel $f_{\mathbf{v}}(\mathbf{n})$ that has limited spatial support [38]. For instance, Fig. 9 shows a function $f_{\mathbf{v}}(\mathbf{n})$ defined over a grid of $N_v \times N_v$ points with $N_v = 10$. In this case, the actual complexity of the estimation algorithm is in the order of $N N_v I$. This complexity can be further decreased by reducing the set of states used for pdf computation to those positions that are in the area surrounding the current MT position (i.e., by pdf windowing).

Further modifications of the HMM definition (still preserving the Markov chain assumptions for $\mathbf{q}_i$ and $\mathbf{s}_i$) and

$$\gamma_i(\mathbf{x}_i) = \begin{cases} \mu_0 \, p(\mathbf{y}_0 \,|\, \mathbf{x}_0) p(\mathbf{x}_0) & i = 0 \\ \mu_i \, p(\mathbf{y}_i \,|\, \mathbf{x}_i) \sum_{\mathbf{x}_{i-1} \in \mathcal{X}_0} p(\mathbf{x}_i \,|\, \mathbf{x}_{i-1}) \gamma_{i-1}(\mathbf{x}_{i-1}) & i = 1, 2, \ldots, I-1 \end{cases} \tag{41}$$

the state-sequence estimation can be carried out to improve localization efficiency by reformulating the localization model as a Jump Markov system (JMS) [39], [40]. According to this approach, it is possible to introduce a nonstationary HMM $\boldsymbol{\lambda}_i^{(q)} = \{\boldsymbol{\pi}^{(q)}, \mathbf{A}^{(q)}, \mathbf{B}_i^{(q)}\}$ having state $\mathbf{q}_i \sim \mathcal{MC}(\boldsymbol{\pi}^{(q)}, \mathbf{A}^{(q)})$, and observation pdfs $\mathbf{B}_i^{(q)} = \{p(\mathbf{y}_i \,|\, \mathbf{q}_i, \mathbf{s}_i)\}$ that change over the time i depending on the driving sight chain $\mathbf{s}_i \sim \mathcal{MC}(\boldsymbol{\pi}^{(s)}, \mathbf{A}^{(s)})$. The use of a JMS allows to separate the position state $\mathbf{q}_i$ from the sight state $\mathbf{s}_i$, instead of dealing with the joint position-sight state, thus reducing the cardinality of the state set from $2^L N_1 N_2$ to $N_1 N_2$. In addition, a more efficient sampling of the state space may be introduced by means of particle filtering (PF) techniques [41], [42], that do not require uniform sampling over the grid $\mathcal{Q}$. The dimensions of the measurement set can also be reduced, by using as observation for the HMM the received power only (i.e., a scalar measurement) instead of the RSS profile (i.e., a $K \times 1$ vector), as shown for WLAN in [16] and for WSN in [27]. A PF approach based on scalar RSS measurements for localization in WSN can be found in [27].

C. Parameter Estimation

In realistic scenarios, only partial *a priori* information about the HMM parameter set $\boldsymbol{\lambda} = \{\boldsymbol{\pi}, \mathbf{A}, \mathbf{B}\}$ is available. To efficiently apply the D/TA in practical systems, these parameters have to be estimated by a training procedure that optimally adapts the model $\boldsymbol{\lambda}$ to some observed data $\mathbf{y}_{0:I-1}$. In our specific framework, $\boldsymbol{\lambda}$ depends on few parameters only: the initial state probabilities $\boldsymbol{\pi}$; the position-transition probabilities ϑ (trajectory initiation probability), ν (trajectory termination probability) and $f_{\mathbf{v}}(\mathbf{n})$ (pdf of the 2-D motion driving process); the sight-transition probabilities p_0 and p_1; the parameters defining the wireless channel model, namely τ_{rms} (channel delay spread), α (path-loss exponent), and η_{ref} (SNR). The initial-state distribution can be chosen as described in Section IV.A. As far as the environment-dependent parameters τ_{rms} and α are concerned, realistic values can be drawn from several experimental studies carried out in the literature to characterize different indoor/outdoor scenarios [32], [33], [36]. The sight/position transition probabilities obviously depend on the specific type of MT motion and on the geometrical layout in which the motion takes place. Pdf adjustment to the specific physical system can be accomplished by training and/or by exploiting *a priori* information about the layout geometry whenever available. For instance, the knowledge of the layout planimetry enables the creation of LOS/NLOS maps for each AP making the sight state $\mathbf{s}_i$ known for each spatial position in $\mathcal{Q}$. This can be used to reduce the complexity. In fact, on one hand, the combined HMM state simplifies to the position only (i.e., $\mathbf{x}_i = \mathbf{q}_i$) and the observation pdf can be obtained from either (22) or (23) depending on the $\mathbf{s}_i$ value. On the other hand, it may also be used to improve the accuracy of the D/TA localization. Geometrical constraints could also be used to avoid forbidden transitions of position (e.g., through walls) by defining a nonhomogeneous HMM with transition probabilities depending on the specific position.

To adjust the model parameters $\boldsymbol{\lambda}$, here we employ a training approach that maximizes the probability $p(\mathbf{y}_{0:I-1} \,|\, \boldsymbol{\lambda})$ of an observed training sequence $\mathbf{y}_{0:I-1}$ of length I given the model $\boldsymbol{\lambda}$. A method to analytically derive the maximum likelihood estimate

$$\boldsymbol{\lambda}^* = \arg\max_{\boldsymbol{\lambda}} p(\mathbf{y}_{0:I-1} \,|\, \boldsymbol{\lambda}) \tag{42}$$

is not known. On the other hand, we can select $\boldsymbol{\lambda}$ to locally maximize the likelihood function $p(\mathbf{y}_{0:I-1} \,|\, \boldsymbol{\lambda})$ through an iterative procedure known in the HMM literature as the *Baum-Welch algorithm* [23]. It is an expectation-maximization (EM) technique that, starting from an estimate $\boldsymbol{\lambda}^{(j)}$ at iteration j, evaluates the *a posteriori* probabilities of state occurrence/transition, given the observed sequence $\mathbf{y}_{0:I-1}$. These *a posteriori* pdfs, obtained under the assumption $\boldsymbol{\lambda} = \boldsymbol{\lambda}^{(j)}$, are then used to reestimate the HMM parameters by approximating the probabilities contained in $\boldsymbol{\lambda}$ as expected frequencies of state occurrence/transition (i.e., the reestimation step). The new parameter set $\boldsymbol{\lambda}^{(j+1)}$ is such that

$$p(\mathbf{y}_{0:I-1} \,|\, \boldsymbol{\lambda}^{(j+1)}) \geq p(\mathbf{y}_{0:I-1} \,|\, \boldsymbol{\lambda}^{(j)}). \tag{43}$$

The procedure stops to the parameter set $\boldsymbol{\lambda}_{\mathrm{EM}}$ when the convergence is reached or some limiting criterion is met. Being a local algorithm only, global convergence is not guaranteed and the quality of the solution $\boldsymbol{\lambda}_{\mathrm{EM}}$ strongly depends on the chosen initial parameter set (i.e., a certain and unpredictable bias is present, such that $\mathrm{E}[\boldsymbol{\lambda}_{\mathrm{EM}}] \neq \boldsymbol{\lambda}^*$).

It is important noticing that, in our localization approach, not every parameter needs to be estimated. In fact, as it will become apparent in Section V-A, D/TA performances are rather insensitive to large variations of τ_{rms} and η. We thus select for estimation only the transition probabilities that compose matrix $\mathbf{A}$ or, equivalently, the pdf $f_{\mathbf{v}}(\mathbf{n})$ and the LOS/NLOS sight probabilities p_0 and p_1. Moreover, to speed up the computation, at each step of the iterative procedure, during the reestimation procedure of each state-transition probability, we select the *discrete* frequencies of state transitions evaluated by counting the transition occurrences in the MT trajectory estimated by D/TA rather than computing the *continuous* expected value from the *a posteriori* pdf. For instance, let $p_0^{(j)}$ be the estimate for the parameter p_0 indicating the probability of transition from LOS to LOS obtained at the jth iteration. The D/TA is applied to the training sequence $\mathbf{y}_{0:I-1}$ using the parameters $\boldsymbol{\lambda}^{(j)}$ (i.e., including also $p_0^{(j)}$) and yielding the state sequence estimate $\hat{\mathbf{x}}_{0:I-1}^{(j+1)} = (\hat{\mathbf{q}}_{0:I-1}^{(j+1)}, \hat{\mathbf{s}}_{0:I-1}^{(j+1)})$. Then, the estimated sight sequence $\hat{\mathbf{s}}_{0:I-1}^{(j+1)}$ is used to reestimate the parameter p_0 as

$$\hat{p}_0^{(j+1)} = \frac{N_{0\to 0}^{(j+1)}}{N_0^{(j+1)}} \tag{44}$$

by counting the number $N_0^{(j+1)}$ of transitions from the LOS state and the number $N_{0\to 0}^{(j+1)}$ of self-transitions from the LOS state into itself. The parameter p_1 and the pdf $f_{\mathbf{v}}(\mathbf{n})$ are estimated using the same algorithm. The results of such a parameter estimation approach will be shown in Section V-A.

In closing this section, we also observe that, to efficiently adjust the HMM parameters, the statistics of the MT position/sight process during the localization phase must be the same of those observed during the training phase. Even if the MT is characterized by very slow or very quick movements, the HMM localization method is capable of tracking it, provided that the

same behavior is observed during the training phase in order to properly adjust the transition probabilities and allow accurate tracking of the motion. For instance, if movements are episodic, then the transition probabilities for the MT position have a spiky shape, as the one shown in Fig. 9(c), indicating that the MT is likely to remain still. To estimate such a 2-D motion pdf, the training sequence needs to be long enough to observe also the less probable movements.

V. Simulation Results

A. Performance and Sensitivity Analysis for ML Ranging

The HMM localization method presented in Section IV combines the ML approach for ranging and multilateration with tracking of the MT state. We start this performance analysis by focusing on the first method, evaluating the accuracy and the parameter sensitivity of the ML ranging method. To accomplish this task, we consider at first a simplified scenario where a single MT-AP link is simulated ($L = 1$) in LOS condition only ($\forall i\ s_i = s_{i,1} = 0$). In such a situation, the localization problem simply reduces to ranging, being the TOA $\tau_i = \tau_{i,1}$ or, equivalently, the MT-AP distance $d_i = \overline{c}\tau_i \Delta t$, the only parameter to be estimated from the $K \times 1$ measurement vector $\mathbf{y}_i = \mathbf{y}_{i,\ell}$. To further simplify the notation, the link index (ℓ) is dropped. In addition, the TOA value is assumed constant for each measurement, and it is given by $\tau_i = K/2$. The estimate $\hat{\tau}_i$ is obtained by maximizing the likelihood function $p(\mathbf{y}_i|\tau_i = k, s_i = 0) = \Lambda(\mathbf{y}_i, k, 0)$ over $k : \hat{\tau}_i = \arg\max_k \Lambda(\mathbf{y}_i, k, 0)$.

The root mean square error (RMSE) $\mathrm{E}[(\tau_i - \hat{\tau}_i)^2]^{1/2}$ of the TOA estimate is evaluated for SNR $\eta = \sigma_z^2/\sigma_0^2$ ranging from 0 to 24 dB. Measurements are generated according to the signal model described in Section II with length $K = 1000$ samples, sampling frequency $f_s = 10$ GHz and PDP with exponentially decaying power characterized by $\tau_{\mathrm{rms}} = 10$ ns or, equivalently from (13), $\rho \simeq 0.9$. For each SNR value, the RMSE is computed by averaging the squared TOA estimate errors over a data set $\mathbf{y}_{0:I-1}$ of $I = 10^4$ independent measurement outcomes: RMSE $(\eta) = [I^{-1} \sum_{i=0}^{I-1} (\tau - \hat{\tau}_i(\eta))^2]^{1/2}$. The results are shown in Fig. 10(a) (solid line); it can be seen that an estimate error of about 10 samples (1 ns) can be obtained for SNR values around $4 \div 5$ dB, while for higher accuracy, such as RMSE < 1, an SNR value $\eta > 16$ dB is required.

These results are confirmed by a second simulation, shown in Fig. 10, that tests the robustness of ML ranging to mismodeling within the same simplified scenario. Here, we evaluate the sensitivity of the TOA estimate with respect to the SNR η [Fig. 10(a)] and to the delay spread τ_{rms} [Fig. 10(b)]. The RMSE of the mismodeled estimate is evaluated by generating sets of $I = 10^3$ measurements with fixed parameters $\{\eta, \tau_{\mathrm{rms}}\}$ and then estimating the TOA from each signal using values in the set $\{\hat{\eta}, \hat{\tau}_{\mathrm{rms}}\}$ with $\hat{\eta} \neq \eta$ or $\hat{\tau}_{\mathrm{rms}} \neq \tau_{\mathrm{rms}}$. In more details, for the SNR sensitivity analysis shown in Fig. 10(a), we use $\eta = \{2, 6, 10, 14\}$ dB in the measurement generation phase and $\hat{\eta} = 0 \div 24$ dB in TOA estimation. The delay spread value is the same used for both generation and estimation: $\tau_{\mathrm{rms}} = \hat{\tau}_{\mathrm{rms}} =$ 10 ns (i.e., 100 samples). The results shown in Fig. 10(a) confirm that the lowest RMSE is obtained when $\hat{\eta}$ is close to the true value η. A similar approach is followed in Fig. 10(b) for the evaluation of τ_{rms} sensitivity. Signals are generated using $\eta = \{2, 6, 10, 14\}$ dB and $\tau_{\mathrm{rms}} = 10$ ns, while estimation is carried out with $\hat{\eta} = \eta$ and $\hat{\tau}_{\mathrm{rms}} = 5 \div 20$ ns (i.e., $50 \div 200$ samples). It can be noticed from Fig. 10 that the RMSE around $\hat{\eta} \approx \eta$ and $\hat{\tau}_{\mathrm{rms}} \approx \tau_{\mathrm{rms}}$ is quite flat: good performances can be obtained even for rough estimates of these model parameters.

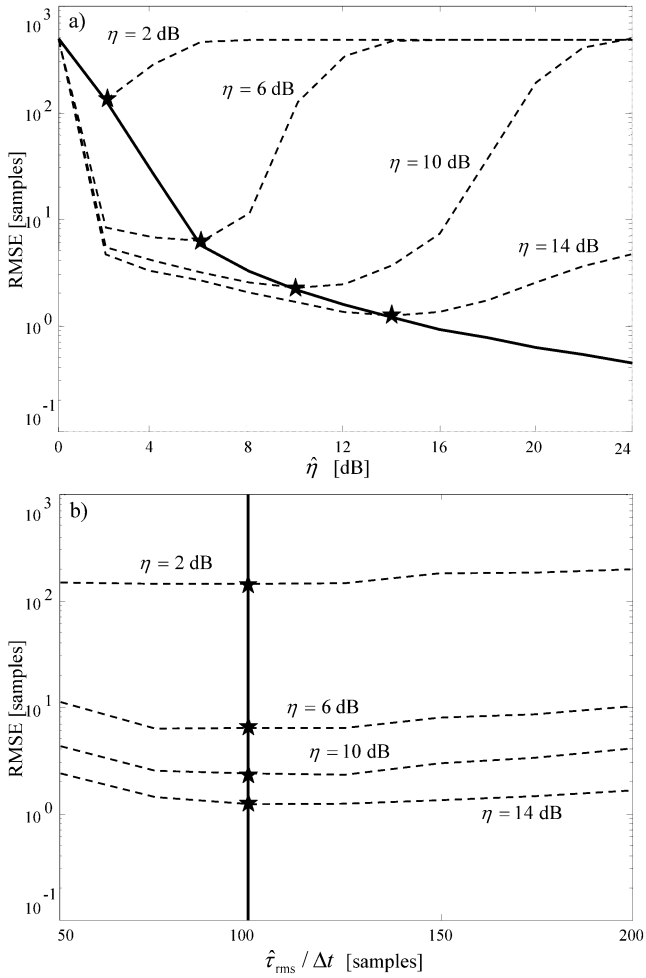

Fig. 10. Sensitivity analysis to parameters η and τ_{rms} (or ρ) in ML ranging. Parameters used for measurement generation are indicated by $\{\eta, \tau_{\mathrm{rms}}\}$, while $\{\hat{\eta}, \hat{\tau}_{\mathrm{rms}}\}$ are those adopted for delay estimation. (a) RMSE as a function of $\hat{\eta}$. (b) RMSE as a function of $\hat{\tau}_{\mathrm{rms}}$. The minimum envelope (corresponding to $\hat{\eta} = \eta$ and $\tau_{\mathrm{rms}} = \hat{\tau}_{\mathrm{rms}}$) is plotted in solid line.

B. ML Ranging in a Multiuser UWB Environment

We extend now the performance analysis for ML ranging considering a more realistic UWB scenario similar to the one described in [19], [43] that is simulated according to the low-bit rate IEEE 802.15.4 standard [22], [44]. TH-BPSK symbols are generated with $N_f = 10$ frames, $N_c = 50$ time slots, $M = 50$ users and randomly assigned TH codes with values $c_j^{(m)}$ uniformly picked in $\{0, 1, \ldots, N_c - 1\}$. The pulse waveform $g_0(t)$ is a Gaussian monocycle with $E_g = 1$ and such that $T_g = 300$ ps. Each transmitted pulse is assumed to be centered in the corresponding time slot, whose duration is $T_c = 2$ ns (i.e., $T_f = 100$ ns). The multipath channel of the mth user, $h^{(m)}(t)$, is modeled according to (7), with chip-spaced delays and exponential PDP $E[|h^{(m)}[\tau(p)]|^2] = \sigma_h^2 \rho^{-p}$; the decaying factor is $\rho =$

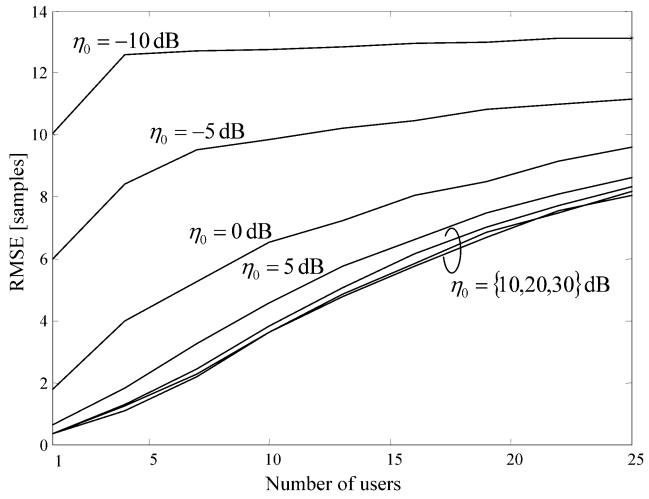

Fig. 11. RMSE of ML ranging as a function of the SNR η_0 and the number of interferers M. The SNR is defined for the single-user single-frame case.

$\exp(-T_c/\tau_{\rm rms})$ with delay spread $\tau_{\rm rms} = 10$ ns; the power σ_h^2 is the same for all users. At the receiver, the discrete-time signal (6) for each user is obtained by matched filtering and frame realignment according to (3), then followed by sampling at chip-rate $\Delta t = T_c$. ML ranging is performed from the obtained signal as described in Section III. We recall that the overall noise power σ_w^2 in (6) is the sum of the background-noise power σ_n^2/N_f and the MAI power from the other users that is proportional to $(M-1)\sigma_h^2$. In the single-user case (i.e., in absence of MAI), the SNR is simply $\eta = N_f\sigma_h^2/\sigma_n^2$ with a gain of $10\log_{10}(N_f) = 10$ dB with respect to the signal before realignment.

Fig. 11 shows the RMSE of the ML ranging vs. the number of users $M = 1,\ldots,25$. Parameter $\eta_0 = \sigma_h^2/\sigma_n^2 \in \{-10,-5,0,5,10,20,30\}$ dB denotes the SNR at the break-point event in signal (6) for the single-user (i.e., $N_u = 1$) single-frame (i.e., $N_f = 1$) case. RMSE values are expressed in terms of time samples and are obtained by averaging over 10^3 channel outcomes. For very low η_0 values (i.e., $\eta_0 \leq -10$ dB), the system performance is dominated by the background noise, the signal-to-interference-noise ratio (SINR) reduces to the SNR $\eta = N_f\sigma_h^2/\sigma_n^2$ and performance is not affected by the number of users. In this case, the error can be considered uniformly distributed within the frame interval and the RMSE reduces to $N_c/\sqrt{12} \simeq 14$ time samples for any M. On the other hand, for increasing η_0, the background noise becomes negligible and MAI critical: for $\eta_0 \geq 10$ dB the SINR is approximately given by $1/(M-1)$ and the RMSE depends only on M (i.e., not on η_0).

C. Localization Performance in a Simplified Environment

At first, performance evaluation is carried out by simulating a MT traveling within a circular layout (with diameter $D = 30$ m and spatial sampling interval $\Delta q = 0.5$ m) that communicates with $L = 3$ APs placed on the border of the area. Changes of the MT location over the time are simulated according to the Gaussian-shaped pdf $f_{\mathbf{v}}(\mathbf{n})$ shown in Fig. 9(a), with $\sigma_v = 3$ space samples. The HMM is assumed to be always in tracking mode (i.e., $\vartheta = 1$ and $\nu = 0$). The sight conditions $\{s_{i,\ell}\}_{\ell=1}^3$ are simulated by exploiting three independent homogeneous first-order Markov chains, according to the model described in Section IV-A. Measurements $\mathbf{y}_{i,\ell}$, sampled at $f_s = 1$ GHz, have length $K = 150$, with the first arrival delay $\tau_{i,\ell}$ being obtained from the MT-AP distance as $\tau_{i,\ell} = \|\mathbf{q}_i - \mathbf{q}_{{\rm AP}\ell}\|/\overline{c}$ and the additional NLOS delay $\delta_{i,\ell}$ having discrete exponential pdf $f_\delta(k) \propto \sigma_\delta^{-1}\exp(-k/\sigma_\delta)$ with $\sigma_\delta = 10$. The PDP of each signal is generated according to the model described in Section II: the peak power (or, equivalently, the SNR $\eta(\tau)$) is calculated as indicated by the path-loss law (14) with exponent $\alpha = 2.4$, while the exponential PDP is simulated with $\rho = 0.9$ ($\tau_{\rm rms} = 10$ ns). The SNR at the reference distance $d_{\rm ref} = 2$ space samples (i.e., 1 m) is $\eta_{\rm ref} = 40$ dB.

The algorithm performances are evaluated in terms of RMSE of the location estimate $\hat{\mathbf{q}}_i$ as a function of the spatial position $\mathbf{n}$ over a trajectory of $I = 3\times 10^4$ steps that covers the whole layout area $\mathcal{Q}$. For a given position $\mathbf{n} \in \mathcal{Q}$, the estimate error is computed as: ${\rm RMSE}(\mathbf{n}) = \{|\mathcal{I}(\mathbf{n})|^{-1}\sum_{i\in\mathcal{I}(\mathbf{n})}\|\mathbf{q}_i - \hat{\mathbf{q}}_i\|^2\}^{1/2}$, where $\mathcal{I}(\mathbf{n}) = \{i : \mathbf{q}_i = \mathbf{n}\}$ is the set of all time instants in which the trajectory flows across $\mathbf{n}$ and $|\mathcal{I}(\mathbf{n})|$ is its cardinality (i.e., the number of times the location $\mathbf{n}$ is visited).

A first example of MT tracking is shown in Fig. 12(a) and (b), where, for visualization purposes only, the MT trajectory is forced to be smoother and shorter: $I = 50$. The dashed area close to each AP is not used. Sight processes are simulated using the following sight parameters: $p_0 = p_1 = 0.7$. These figures compare the true trajectories (thick line) with the estimated ones (markers) obtained by local MLE [Fig. 12(a)] or D/TA [Fig. 12(b)]. Estimate errors can be appreciated by looking at the short segments that connect the true position to the corresponding estimated one. False positioning events occur when using local MLE only.

More details about the delay estimates $\hat{\tau}_{i,\ell} = \|\hat{\mathbf{q}}_i - \mathbf{q}_{{\rm AP}\ell}\|/\overline{c}$, obtained according the D/TA location estimate $\hat{\mathbf{q}}_i$, are shown in Fig. 13. For each MT-AP link, the true propagation time over the LOS distance $d_{i,\ell}/\overline{c}$ (solid line), the first arrival delay (dashed line) and the D/TA delay estimate (markers) are plotted versus the position index along the trajectory. The plot below each figure shows the LOS or NLOS sight conditions experienced (solid line) and estimated (markers) along the trajectory. The bias of the distance due to multipath is effectively compensated by the D/TA algorithm.

Figs. 14 and 15 show the RMSE of the estimate as a function of the position $\mathbf{n} \in \mathcal{Q}$ for a) the local MLE and b) the D/TA methods. The performances are evaluated in LOS-only conditions, with $p_0 = 1$ and $p_1 = 0$ (Fig. 14), and in mixed LOS/NLOS conditions, with $p_0 = p_1 = 0.7$ (Fig. 15). In the MLE-LOS map, the error increases near the APs, while it is quite uniform in the middle of the layout. This effect is due to false positioning errors occurring when one or more measurements $\mathbf{y}_{i,\ell}$ refer to a distant AP [7]. These problems are solved by the D/TA which yields a uniform error map all over the layout. The advantage of the D/TA, especially in mixed LOS/NLOS conditions, is more evident in Figs. 14(c) and 15(c), which show the vertical sections for $\{n_1 = 0\}$ of the maps in Figs. 14(a)–(b) and 15(a)–(b), respectively. The local MLE yields very poor performance, with RMSE ranging from 0 to 30 space samples, while the D/TA error is stable under five samples, in both LOS and mixed LOS/NLOS cases.

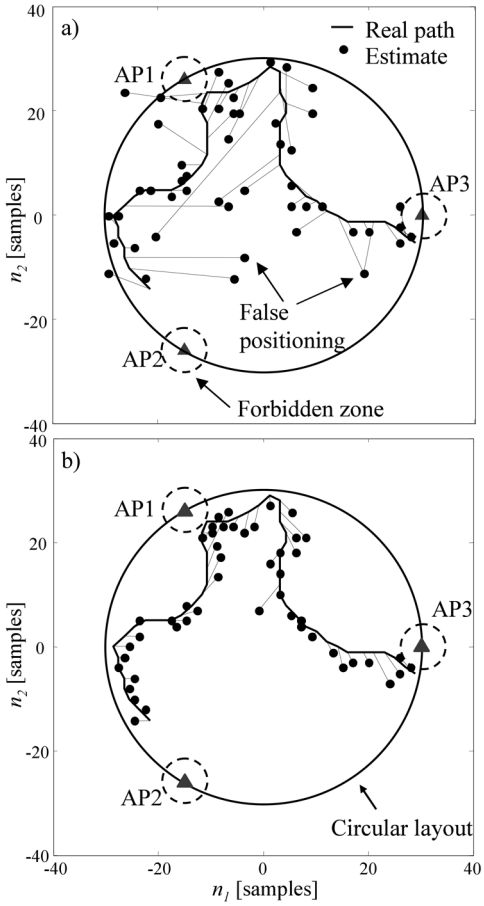

Fig. 12. Examples of localization with local MLE (a) and D/TA (b) within a simplified circular layout (the dashed area close to each AP is not used). The solid line indicates the true trajectory $\{\mathbf{q}_i\}$ while the markers show the estimates. True positions and corresponding estimates are related by a short segment.

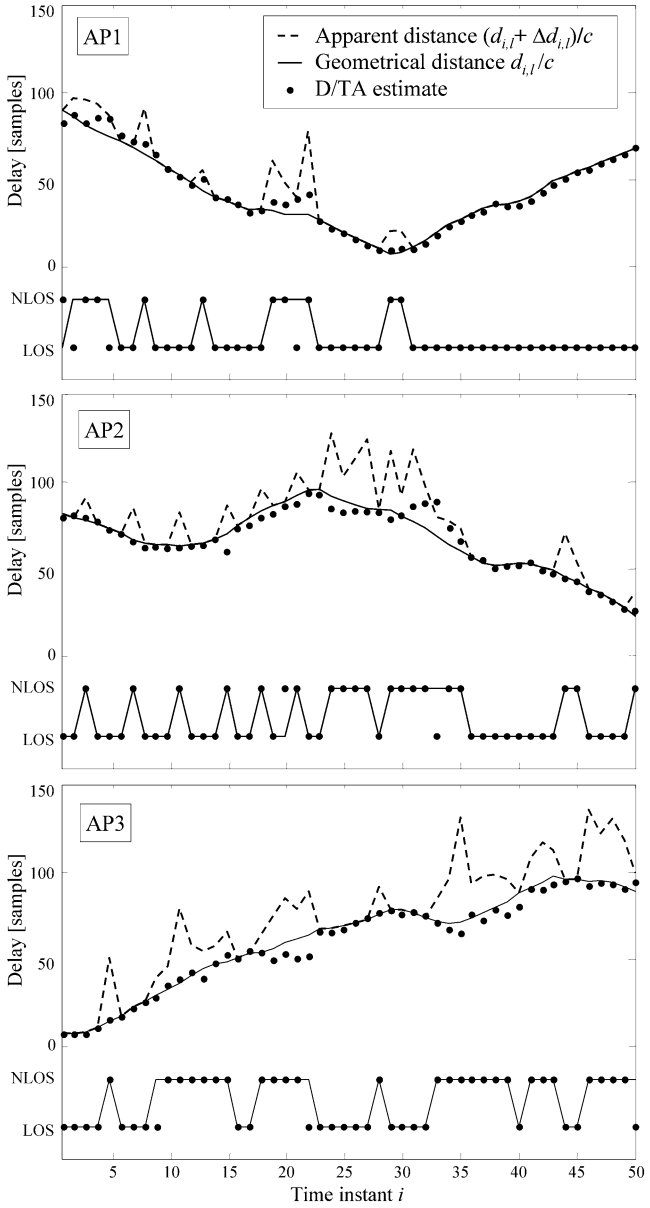

Fig. 13. Estimation of MT-AP distance/delay (upper part of each figure) and sight condition (lower part of each figure) for all $L = 3$ links as summarized in the example in Fig. 12.

Finally, the position RMSE versus the reference SNR η_{ref} is shown in Fig. 16. For the same localization scenario adopted in the previous examples, a trajectory of $I = 10^4$ positions is generated for each value of η_{ref}. We recall that, even if η_{ref} is fixed, the SNR is nonuniform across the space $\mathcal{Q}$, as the received signal power varies with the MT position due to the path-loss. Only in the ideal case $\alpha = 0$ (absence of path-loss) the SNR is constant for all positions. In this experiment, the following cases are considered: $\alpha = 0$ with $\eta_{\text{ref}} = -10 \div 20$ dB [Fig. 16(a)] and $\alpha = 2.4$ with $\eta_{\text{ref}} = 20 \div 60$ dB [Fig. 16(b)]. These figures compare the localization accuracy for local MLE and D/TA methods. The error floor at very low and very large SNR is determined by the finite value of the temporal support of each measurement and the spatial sampling interval, respectively. The performance gain provided by D/TA for intermediate SNR values is around $12 \div 13$dB in presence of path-loss. Notice that the error curve in Fig. 16 coincides with the envelope of the minima $(\eta = \hat{\eta})$ of the simulation in Fig. 10(a).

D. Parameter Estimation and Sensitivity Analysis

As pointed out in Section IV, the proposed HMM approach exploits the ML technique for ranging and multilateration while tracking the MT state. The robustness of the ML ranging algorithm with respect to parameter mismodeling for $\{\eta, \tau_{\text{rms}}\}$ has been investigated in the simulation of Fig. 10. In this paragraph, we extend these considerations to include also the sensitivity analysis for the HMM state-transition probabilities. For these simulations, we assume the same localization scenario illustrated in Section V-C. The tracking-algorithm sensitivity to the parameter σ_v (i.e., the standard deviation of the 2-D Gaussian distribution $f_{\mathbf{v}}(\mathbf{n})$) is studied using the following parameters: $\sigma_v = \{1, 2, 3, 4\}$ for the HMM generation and $\hat{\sigma}_v = 0.5 \div 6.5$ for the state-sequence estimation. For each pair $(\sigma_v, \hat{\sigma}_v)$, Fig. 17 shows the RMSE of the location estimate evaluated over a MT trajectories of length $I = 2 \cdot 10^3$. Both mixed LOS/NLOS [Fig. 17(a)] and LOS only [Fig. 17(b)] conditions are simulated. It is apparent from Fig. 17(b) that in LOS only conditions the

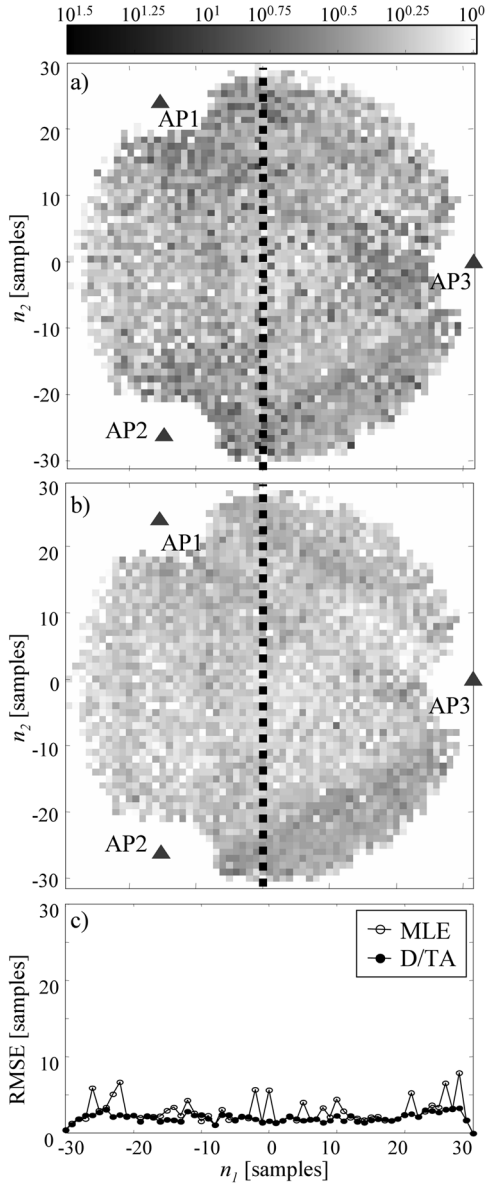

Fig. 14. RMSE versus MT position in LOS-only conditions. (a) MLE position estimate. (b) D/TA position estimate. (c) Section $\{n_1 = 0\}$ from maps in (a) and (b).

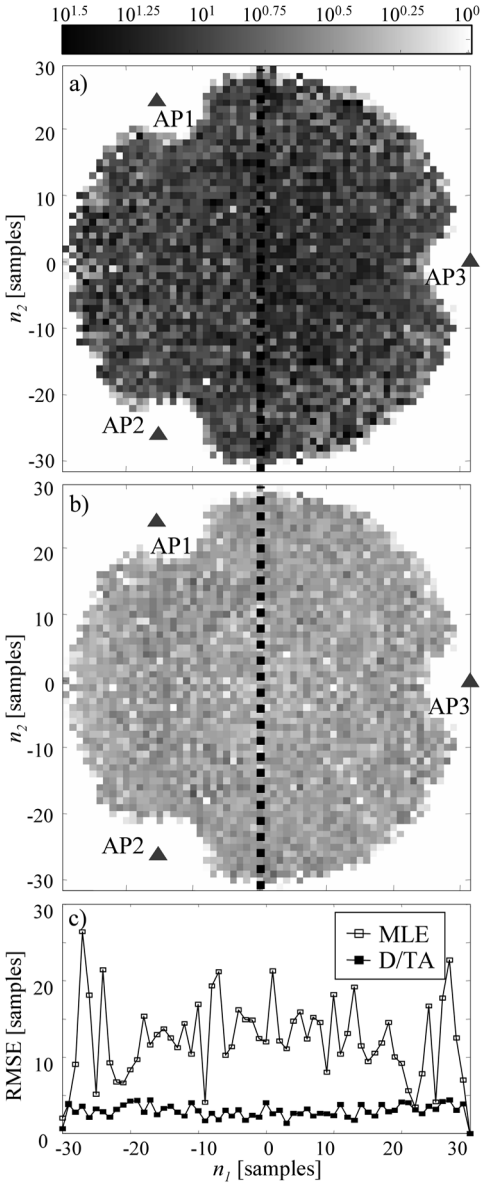

Fig. 15. RMSE versus MT position in mixed LOS/NLOS conditions. (a) MLE position estimate. (b) D/TA position estimate. (c) Section $\{n_1 = 0\}$ from maps in (a) and (b).

optimum parameter choice is $\hat{\sigma}_v = \sigma_v$. In addition, due to the flatness of the RMSE curves, if inaccurate information about σ_v are available, it is preferable to overestimate it. However, as depicted in Fig. 17(a), this does not hold true in LOS/NLOS conditions since the optimum parameter choice is related to the joint position-sight variable $(\mathbf{q}_i, \mathbf{s}_i)$ and not only to the position variable $\mathbf{q}_i$ as in the previous case. Moreover, the RMSE positioning error is greater with respect to the one in the LOS only case. In the LOS/NLOS scenario, it is convenient to choose $\hat{\sigma}_v \leq \sigma_v$, since the optimum choice $\hat{\sigma}_v$ is close to the true value σ_v and the curves are quite flat around the optimum values denoting moderate mismodeling errors.

HMM parameter estimation is carried out by the iterative procedure discussed in Section IV-C for a training sequence of $I = 10^4$ steps. Measurements are simulated using the same parameters introduced in Section V-C except for p_0 and p_1 that are assigned as: $p_0 = 0.25$ and $p_1 = 0.75$ (i.e., high probability to have NLOS conditions). The HMM model $\boldsymbol{\lambda}^{(1)}$ employed in the iterative procedure is initialized with a uniform transition distribution $f_{\mathbf{v}}^{(1)}(\mathbf{n})$ (defined over a 21×21 square grid) and with $p_0^{(1)} = p_1^{(1)} = 0.5$. As shown in Fig. 18(a) and (b), convergence of both the location transition probability $f_{\mathbf{v}}(\mathbf{n})$ and the sight transition probabilities $\{p_0, p_1\}$ to realistic values is accomplished in very few iterations. A small amount of bias can be noticed in the estimates of p_0 and p_1; as aforementioned in Section IV-C, this is due to the fact that, to reduce the computational complexity, the statistics along the i coordinate were computed using the estimated sequence $\{\hat{\mathbf{x}}_i\}$ rather than exploiting the statistics of the *a posteriori* pdf sequence $\{\gamma(\mathbf{x}_i)\}$.

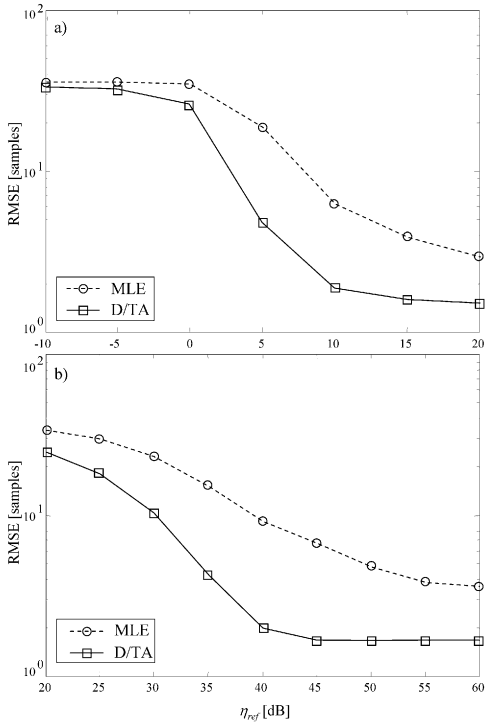

Fig. 16. RMSE of the position estimate versus the reference SNR η_{ref} for MLE and D/TA. (a) Absence of path-loss ($\alpha = 0$). (b) Realistic indoor attenuation ($\alpha = 2.4$).

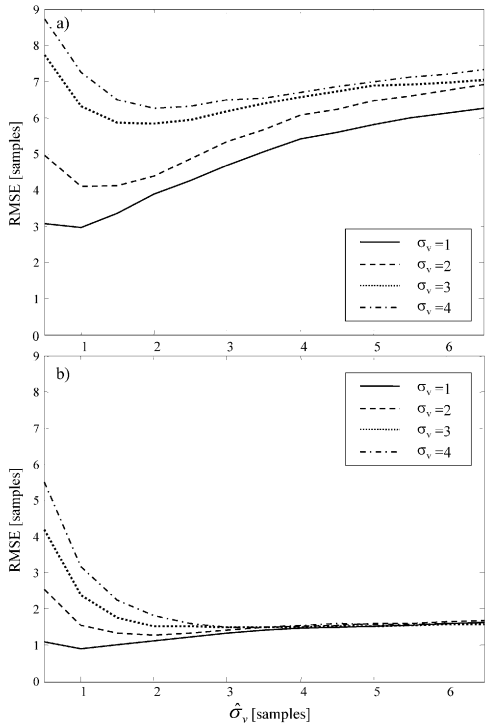

Fig. 17. Sensitivity analysis for the HMM algorithm to parameter σ_v. The parameter used for measurement generation is indicated by σ_v while $\hat{\sigma}_v$ is the one adopted for tracking. The RMSE is plotted as a function of $\hat{\sigma}_v$. (a) In mixed LOS/NLOS conditions. (b) In LOS only.

E. Localization in Realistic Indoor Environments

In a different way with respect to the simplified localization experiments so far considered, in real environments the sight process is inevitably correlated to the MT position. This is taken into account in the indoor scenario sketched in Fig. 5, consisting in a rectangular layout of 40×30 m (i.e., $N_1 = 61$ and $N_2 = 81$ with sampling interval $\Delta q = 50$ cm), with walls, doors and $L = 4$ APs. The MT trajectory is generated, within this layout, using a conic-shaped pdf $f_{\mathbf{v}}(\mathbf{n})$ [see Fig. 9(c)], having base with radius of $\varepsilon = 4$ space samples. In the generation phase, the sight conditions are calculated according to the specific layout by ray tracing from each MT position to the four AP positions (NLOS condition occurs when a wall is between an AP and the MT). The resulting LOS/NLOS maps, or coverage maps, used for measurement generation are shown in Fig. 19; the gray scale indicates, for

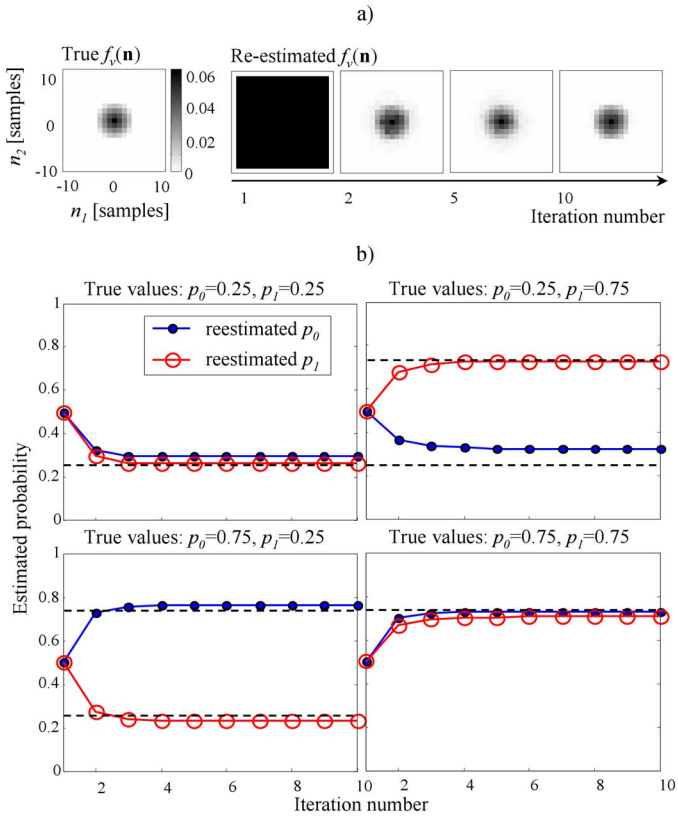

Fig. 18. Convergence in the Baum-Welch estimate of transition probabilities $f_{\mathbf{v}}(\mathbf{n})$ for positions and $\{p_0, p_1\}$ for sights. (a) True and reestimated pdf $f_{\mathbf{v}}(\mathbf{n})$ (a conic-shaped distribution is simulated as in Fig. 9(c). (b) Reestimation sequences for $p_0, p_1 \in \{0.25, 0.75\}$.

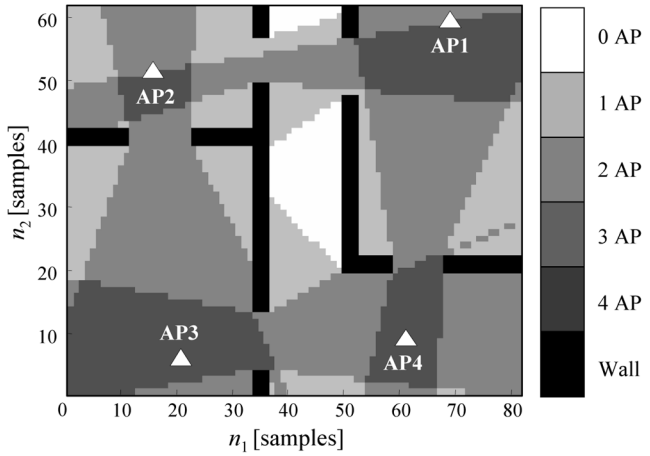

Fig. 19. Coverage maps for the localization scenario of Fig. 5.

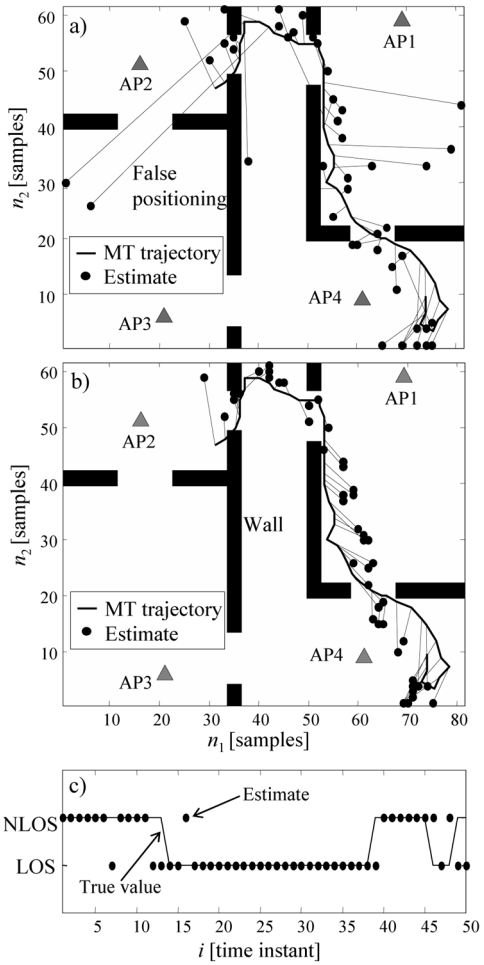

Fig. 20. Example of trajectory tracking in a realistic indoor scenario with walls, doors, and 4 APs. (a) MLE estimate. (b) D/TA position estimate. (c) D/TA sight estimate for AP1.

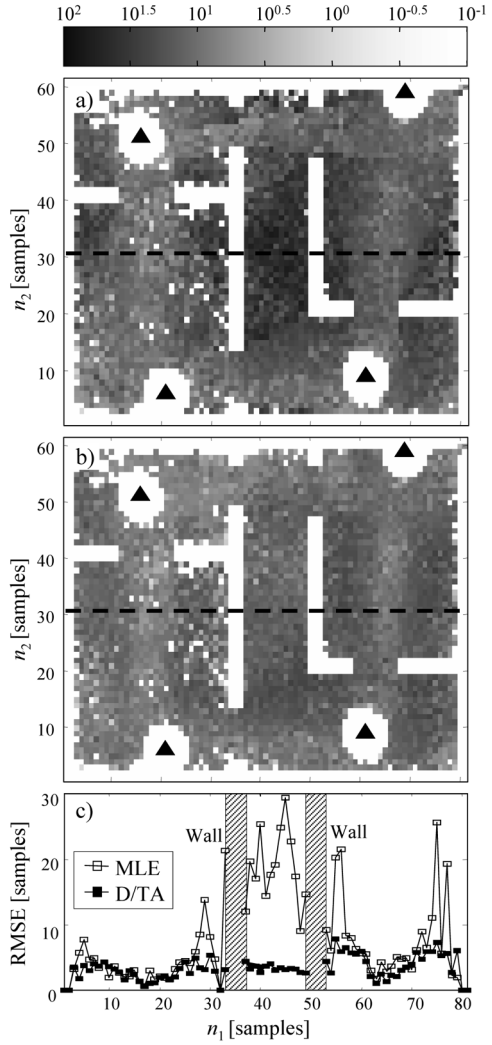

Fig. 21. RMSE versus MT position in a realistic indoor scenario with mixed LOS/NLOS conditions. (a) MLE position estimate. (b) D/TA position estimate. (c) Section $\{n_2 = 31\}$ from maps in (a) and (b).

each spatial position, the number of APs that are LOS linked to that position. The fact that position and sight are no longer independent does not really affect the HMM localization, where the estimates are jointly performed as usual. To select the $\{p_0, p_1\}$ values to be used in this model, we have generated a training trajectory of $I = 2 \times 10^4$ steps across the considered layout and we have estimated $\{p_0, p_1\}$ through the statistics of the corresponding LOS/NLOS state changes. The results obtained by this procedure are $p_0 \simeq p_1 \simeq 0.9$ (lower values might be obtained in the same layout by generating randomly placed obstacles that simulate people and other field scatterers). The other parameters used for this simulation are: sampling frequency $f_s = 1$ GHz, measurement length $K = 150$, mean excess delay $\sigma_\delta = 10$, path-loss exponent $\alpha = 2.4$, reference SNR $\eta_{\text{ref}} = 40$ dB at $d_{\text{ref}} = 2$ and PDP decaying factor $\rho = 0.9$ ($\tau_{\text{rms}} = 10$ ns).

An example of trajectory estimation is shown in Fig. 20; for further details about this simulation the reader can refer to the example in Fig. 13 for the simplified localization environment. It is apparent here how MT tracking can effectively reduce false localizations in poorly covered areas (e.g., in the central corridor). The plot in Fig. 20(c) compares the true value (line) and the D/TA estimate (circles) of the sight condition over the MT-AP1 link.

Fig. 21(a) and (b) plot the RMSE maps as a function of the MT position for both MLE and D/TA estimates. RMSE values are obtained by averaging over a trajectory of $I = 4 \times 10^4$ steps. These maps let us appreciate how D/TA improves the estimate performances in almost the whole layout. As indicated by the RMSE map in Fig. 21(a), the central corridor is critical for the memory-less approach used by the local MLE algorithm, because every MT-AP link is in NLOS. The filtering and prediction capabilities of the D/TA Bayesian approach are especially useful in these NLOS situations, where a dramatic improvement can be achieved [e.g., see the slice $n_2 = 31$ in Fig. 21(c)] with respect to the local MLE.

VI. Conclusion

A novel approach has been proposed to track the location of MTs in order to alleviate the NLOS problem that arises in dense multipath indoor conditions. Local ML algorithms introduce tracking errors since they do not take into account the physical constraints due to MT trajectory. On the contrary, the D/TA algorithm here proposed is based on a HMM Bayesian approach that models the MT moving capabilities. To further reduce tracking

errors due to mixed LOS/NLOS conditions, the proposed algorithm jointly estimates both position and sight conditions of the MT. Its tracking capabilities have been at first evaluated in a simple scenario and they have been compared to the performance of a local ML algorithm. Then both algorithms have been assessed in a more realistic UWB environment. Simulations show that performances achieved by keeping into consideration mixed LOS/NLOS conditions for all radio links are similar to those obtained in an ideal LOS propagation environment.

REFERENCES

[1] G. Sun, J. Chen, W. Guo, and K. J. R. Liu, "Signal processing techniques in network-aided positioning: A survey of state-of-the-art positioning designs," *IEEE Signal Process. Mag.*, vol. 22, no. 4, pp. 12–23, Jul. 2005.

[2] A. H. Sayed, A. Tarighat, and N. Khajehnouri, "Network-based wireless location," *IEEE Signal Process. Mag.*, vol. 22, no. 4, pp. 24–40, Jul. 2005.

[3] F. Gustafsson and F. Gunnarsson, "Mobile positioning using wireless networks," *IEEE Signal Process. Mag.*, vol. 22, no. 4, pp. 41–53, Jul. 2005.

[4] N. Patwari, J. N. Ash, S. Kyperountas, A. O. Hero III, R. L. Moses, and N. S. Correal, "Localizating the nodes," *IEEE Signal Process. Mag.*, vol. 22, no. 4, pp. 54–69, Jul. 2005.

[5] S. Gezici, Z. Thian, G. B. Giannakis, H. Kobayashi, A. F. Molisch, H. V. Poor, and Z. Sahinoglu, "Localization via ultra-wideband radios," *IEEE Signal Process. Mag.*, vol. 22, no. 4, pp. 70–84, Jul. 2005.

[6] J. J. Caffrey and G. L. Stuber, "Overview of radiolocation in CDMA cellular systems," *IEEE Commun. Mag.*, vol. 36, no. 4, pp. 38–45, Apr. 1998.

[7] N. R. Yousef, A. H. Sayed, and L. M. A. Jalloul, "Robust wireless location over fading channels," *IEEE Trans. Veh. Technol.*, vol. 52, no. 1, pp. 117–126, Jan. 2003.

[8] T. Roos, P. Myllymaki, and H. Tirri, "A statistical modeling approach to location estimation," *IEEE Trans. Mobile Comput.*, vol. 1, no. 1, pp. 59–69, Jan.–Mar. 2002.

[9] A. Howard, S. Siddiqi, and G. S. Sukhatme, "An experimental study of localization using wireless Ethernet," in *Proc. 4th Int. Conf. Field and Service Robotics (FSR 2003)*, Jul. 2003.

[10] J.-Y. Lee and R. A. Scholtz, "Ranging in a dense multipath environment using an UWB radio link," *IEEE J. Sel. Areas Commun.*, vol. 20, no. 9, pp. 1677–1681, Dec. 2002.

[11] N. Patwari, A. O. Hero III, M. Perkins, N. S. Correal, and R. J. O. Dea, "Relative location estimation in wireless sensor networks," *IEEE Trans. Signal Process.*, vol. 51, no. 8, pp. 2137–2148, Aug. 2003.

[12] Z. Sahinoglu and A. Catovic, "A hybrid localization estimation scheme (H-LES) for partially synchronized wireless sensor networks," in *Proc. IEEE Int. Conf. Commun. (ICC 2004)*, Jun. 2004, vol. 7, pp. 3797–3801.

[13] A. Urruela and J. Riba, "Efficient mobile location from time measurements with unknown variances in dynamic scenarios," in *Proc. IEEE Workshop Signal Process. Adv. Wireless Commun. (SPAWC 2004)*, Jul. 2004, pp. 571–575.

[14] C. D. Wann and M. H. Lin, "Data fusion methods for accuracy improvement in wireless location systems," in *Proc. IEEE Wireless Commun. Networking Conf. (WCNC 2004)*, Mar. 2004, vol. 1, pp. 471–476.

[15] B. L. Mark and Z. R. Zaidi, "Robust mobility tracking for cellular networks," in *Proc. IEEE Int. Conf. Commun. (ICC 2002)*, May 2002, vol. 1, pp. 445–449.

[16] V. Seshadri, G. V. Zaruba, and M. Huber, "A Bayesian sampling approach to in-door localization of wireless devices using received signal strength indication," in *Proc. IEEE Int. Conf. Pervasive Comput. Commun. (PerCom 2005)*, Mar. 2005, pp. 75–84.

[17] C. D. Wann, Y. M. Chen, and M. S. Lee, "Mobile location tracking with NLOS error mitigation," in *Proc. IEEE Global Telecommun. Conf. (IEEE GLOBECOM 2002)*, Nov. 2002, vol. 2, pp. 1688–1692.

[18] M. Nàjar and J. Vidal, "Kalman tracking for mobile location in NLOS situations," in *Proc. IEEE Int. Symp. Pers., Indoor, Mobile Radio Commun. (PIMRC 2003)*, Sep. 2003, pp. 2203–2207.

[19] M. Z. Win and R. A. Scholtz, "Ultra-wide bandwith time-hopping spread-spectrum impluse radio for wireless multiple-access communications," *IEEE Trans. Commun.*, vol. 48, no. 4, pp. 679–691, Apr. 2000.

[20] F. Ramirez-Mirales, "Performance of ultrawideband SSMA using time hopping and *M*-ary PPM," *IEEE J. Sel. Areas Commun.*, vol. 19, no. 6, pp. 1186–1196, Jun. 2001.

[21] *IEEE Standard for Information Technology—Telecommunications and Information Exchange Between Systems—Local and Metropolitan Area Networks Specific Requirements Part 15.3: Wireless Medium Access Control (MAC) and Physical Layer (PHY) Specifications for High Rate Wireless Personal Area Networks (WPANs)*, IEEE Standard 802.15.3-2003.

[22] *IEEE Standard for Information Technology—Telecommunications and Information Exchange Between Systems—Local and Metropolitan Area Networks Specific Requirements Part 15.4: Wireless Medium Access Control (MAC) and Physical Layer (PHY) Specifications for Low-Rate Wireless Personal Area Networks (LR-WPANs)*, IEEE Standard 802.15.4-2003.

[23] L. R. Rabiner, "A tutorial on hidden Markov models and selected applications in speech recognition," *Proc. IEEE*, vol. 77, no. 2, pp. 257–286, Feb. 1989.

[24] C. Morelli, M. Nicoli, V. Rampa, and U. Spagnolini, "Hidden Markov models for radio location of moving terminals in LOS/NLOS conditions," in *Proc. IEEE Int. Conf. Acoust, Speech, Signal Process. (ICASSP 2005)*, Mar. 2005, vol. 4, pp. 877–880.

[25] M. Nicoli, V. Rampa, and U. Spagnolini, "Hidden Markov model for multidimensional wavefront tracking," *IEEE Trans. Geosci. Remote Sens.*, vol. 40, no. 3, pp. 651–655, Mar. 2002.

[26] C. Mazzucco, U. Spagnolini, and G. Mulas, "A ranging technique for UWB indoor channel based on power delay profile analysis," in *Proc. IEEE Veh. Technol. Conf. (VTC 2004 Spring)*, May 2004, vol. 5, pp. 2595–2599.

[27] C. Morelli, M. Nicoli, V. Rampa, and U. Spagnolini, "Particle filters for RSS-based localization in wireless sensor networks: An experimental study," in *Proc. IEEE Int. Conf. Acoust, Speech, Signal Process. (ICASSP 2006)*, May 2007, vol. 4, pp. 957–960.

[28] I. Guvenc and H. Arslan, "UWB channel estimation with various sampling rate options," in *IEEE Sarnoff Symp. Adv. Wired and Wireless Commun.*, Apr. 2005, pp. 229–232.

[29] M. Z. Win and R. A. Scholtz, "Ultra-wide bandwidth time-hopping spread-spectrum impulse radio for wireless multiple-access communications," *IEEE Trans. Commun.*, vol. 48, no. 4, pp. 679–691, Apr. 2000.

[30] B. Hu and N. C. Beaulieu, "Accurate evaluation of multiple-access performance in TH-PPM and TH-BPSK UWB systems," *IEEE Trans. Commun*, vol. 52, no. 10, pp. 1758–1766, Oct. 2004.

[31] N. Antoniadis and A. O. Hero III, "Time-delay estimation for filtered Poisson processes using an EM-type algorithm," *IEEE Trans. Signal Process.*, vol. 42, no. 8, pp. 2112–2123, Aug. 1994.

[32] S. S. Ghassemzadeh, L. J. Greenstein, T. Sveinsson, A. Kavcic, and V. Tarokh, "UWB delay profile modeles for residential and commercial indoor environments," *IEEE Trans. Veh. Technol.*, vol. 54, no. 4, pp. 1235–1244, Jul. 2005.

[33] L. J. Greenstein, V. Erceg, Y. S. Yeh, and M. V. Clark, "A new path-gain/delay-spread propagation model for digital cellular channels," *IEEE Trans. Veh. Technol.*, vol. 46, no. 2, pp. 477–485, May 1997.

[34] D. D. McCrady, L. Doyle, H. Forstrom, T. Dempsy, and M. Martorana, "Mobile ranging with low accuracy clocks," *IEEE Trans. Microw. Theory Technol.*, vol. 48, no. 4, pp. 951–957, Jun. 2000.

[35] N. Patwari and A. O. Hero III, "Location estimation accuracy in wireless sensor networks," in *Proc. IEEE Asilomar Conf. Signals, Syst., Comput.*, Nov. 2002, vol. 2, pp. 1523–1527.

[36] M. Dohler, B. Allen, A. Armogida, S. McGregor, M. Ghavami, and A. H. Aghvami, "A novel powerloss model for short range UWB transmissions," *Proc. Conf. Ultrawideband Systems and Technology (UWBST) & Int. Workshop for Ultra Wideband Systems (IWUWBS) 2004*, pp. 81–85, May 2004.

[37] U. Spagnolini and V. Rampa, "Multitarget detection/tracking for monostatic ground penetrating radar: Application to pavement profiling," *IEEE Trans. Geosci. Remote Sens.*, vol. 37, no. 1, pp. 383–394, Jan. 1999.

[38] S. Geman and D. Geman, "Stochastic relaxation, Gibbs distributions, and the Bayesian restoration of images," *IEEE Trans. Pattern Anal. Machine Intell.*, vol. 6, no. 6, pp. 721–741, 1984.

[39] C. Andrieau, M. Davy, and A. Doucet, "Efficient particle filtering for jump Markov systems. Application to time-varying autoregressions," *IEEE Trans. Signal Process.*, vol. 51, no. 7, pp. 1762–1770, Jul. 2003.

[40] A. Logothetis and V. Krishnamurthy, "Expectation maximization algorithms for MAP estimation of jump Markov linear systems," *IEEE Trans. Signal Process.*, vol. 47, no. 8, pp. 2139–2156, Aug. 1999.

[41] M. S. Arulampalam, S. Maskell, N. Gordon, and T. Clapp, "A tutorial on particle filters for online nonlinear/non-Gaussian Bayesian tracking," *IEEE Trans. Signal Process.*, vol. 50, no. 2, pp. 174–188, Feb. 2002.
[42] A. Ooi, B. Vo, and A. Doucet, "Particle filtering for multi-target tracking using jump Markov systems," in *Proc. IEEE Intell. Sens., Sens. Netw. Inf. Process. Conf. (ISSNIP 2004)*, Dec. 2004, pp. 131–136.
[43] M. Z. Win and R. A. Scholtz, "Impulse radio: How it works," *IEEE Commun. Lett.*, vol. 2, no. 2, pp. 36–38, Feb. 1998.
[44] A. F. Molish, K. Balakrishnan, C. Chong, S. Emami, A. Fort, J. Karedal, J. Kunisch, H. Schantz, U. Schuster, and K. Siwiak, "IEEE 802.15.4a channel model 9—Final report," *IEEE 802.15 PHY Task Group 4a*, Nov. 2004.

Carlo Morelli received the M.Sc. degree in telecommunication engineering from the Politecnico di Milano, Milan, Italy, in 2004.

From October 2004 to November 2005, he was with the Digital Signal Processing Group, Dipartimento di Elettronica e Informazione, Politecnico di Milano, as a researcher. He currently works for Siemens S.p.a. in the Research and Development area for point-to-point radio solutions. His research interests involve Bayesian filtering, advanced modulation techniques, and applied information theory.

Monica Nicoli (M'99) received the M.Sc. degree (with honors) and the Ph.D. degree in telecommunication engineering from the Politecnico di Milano, Milan, Italy, in 1998 and 2002, respectively.

During 2001, she was a visiting researcher at Signals and Systems, Uppsala University, Sweden. Currently, she is an Assistant Professor with the Dipartimento di Elettronica e Informazione, Politecnico di Milano. Her research interests are in the area of signal processing for wireless communication systems: antenna arrays processing, MIMO systems, channel estimation and equalization, multiuser detection, turbo processing, multicarrier systems, Bayesian tracking for wireless localization, and remote sensing applications.

Dr. Nicoli received the Marisa Bellisario Award in 1999.

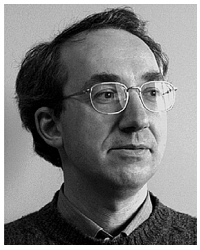

Vittorio Rampa was born in Genoa, Italy, in 1957. He received the Laurea (with honors) as Dottore in Ingegneria Elettronica in 1984 from the Politecnico di Milano, Milan, Italy.

In 1986, he joined the Center for Space Communications (CSTS-CNR) of the Italian National Research Council (CNR) now the Institute of Electronics, Computer and Telecommunication Engineering (IEIIT-CNR) where he is Senior Researcher. He was a Visiting Scholar with the Center for Integrated Systems, Stanford University, Stanford, CA, during 1987–1988. Since 1999, he has also been a Contract Professor with the Politecnico di Milano working in telecommunication architectures. Presently, his research interests include signal processing for telecommunication and radar systems and hardware/software reconfigurable architectures for mobile communication systems.

Umberto Spagnolini (SM'99) received the Dott. Ing. Elettronica (*cum laude*) from the Politenico di Milano, Milan, Italy, in 1988.

Since 1988, he has been with the Dipartimento di Elettronica e Informazione, Politenico di Milano, as an Assistant Professor (1990–1998), an Associate Professor (1998–2006), and a Full Professor (since 2006) in the area of statistical signal processing and communication systems. His general interests are in the area of signal processing, estimation theory, and system identification. The specific areas of interest include channel estimation, array processing and cross-layer optimization (PHY/MAC) for communication systems, parameter estimation and tracking, wavefield interpolation with applications to UWB radar. and remote sensing.

Dr. Spagnolini served as an Associate Editor for the IEEE TRANSACTIONS ON GEOSCIENCE AND REMOTE SENSING from 1999 to 2006. He was awarded the AEI Award (1991), Van Weelden Award of EAGE (1991), and the Best Paper Award from EAGE (1998).